Ultradense protium p(0) and deuterium D(0) and their relation to ordinary Rydberg matter: a review

To cite this article before publication: Leif Holmlid *et al* 2019 *Phys. Scr.* in press https://doi.org/10.1088/1402-4896/ab1276

Ultradense protium p(0) and deuterium D(0) and their relation to ordinary Rydberg matter: a review

Leif Holmlid
Atmospheric Science, Department of Chemistry and Molecular Biology, University of Gothenburg, SE-412 96 Göteborg, Sweden
Email holmlid@chem.gu.se

Sindre Zeiner-Gundersen, Norrønt AS, Vaterlandsveien 19
3470 Slemmestad, Norway
and Science Institute, University of Iceland
Dunhaga 3,107 Reykjavik, Iceland

ABSTRACT:

The extremely large density of ultradense hydrogen H(0) has been proved in numerous experiments by three laser-induced methods, namely Coulomb explosions observed by particle time-of-flight and time-of-flight mass spectrometry (TOF-MS), rotational emission spectroscopy in the visible, and annihilation-like meson ejecting nuclear reaction processes. The density of H(0) at the quite common spin level s=2 is of the order of 100 kg cm^{-3}. The theory of ultradense hydrogen H(0) is described briefly, especially the "mixed" spin quantum number *s* and its relation to the internuclear distances. The orbital angular momentum of the bonding electrons in H(0) is $l = 0$, which gives the H(0) designation. At $s = 2$ with electron total angular momentum $L = \hbar$, the internuclear distance is 2.24 pm, and at $s = 1$ thus $L = \hbar/2$, it is as small as 0.56 pm. The internuclear distances are measured by optical rotational spectroscopy with a precision as good as 10^{-3}, thus with femtometer resolution. The dimensional factor (ratio of internuclear distance to the electron orbit radius) was determined to be 2.9 by electrostatic stability calculations for ordinary Rydberg matter. This value is found to be valid with high precision also for H(0) clusters with different shapes. Superfluidity and a Meissner effect at room temperature are only found for the long chain clusters $H_{2N}(0)$, while the small $H_3(0)$ and $H_4(0)$ clusters do not have any super properties.

Instead, they are the clusters in which most of the nuclear reaction processes take place. These processes give meson showers (most types of kaons and pions) and, after meson decay, large fluxes of muons and other leptons. Published applications of these results already exist in the field of nuclear reactions, energy production (patented fusion reactor), space physics (the solar wind), and in astrophysics (dark matter and the interstellar medium ISM).

PACS: 67.63.Gh, 29.25.-t, 14.40.- n, 13.20.Eb

1. Introduction

The research on ultra-dense hydrogen H(0) which has its most common internuclear distance at 2.3 pm in spin state $s = 2$, falls into several different fields. This means that it may be quite complex to combine the existing information on a certain aspect into a coherent understanding. For this reason, this review attempts to combine this information to make it understandable for example for chemical physicists, for whom the discovery of entirely new types of molecules (clusters) and materials with never before imagined properties may be the most interesting (Holmlid 2013a,b, 2017a,b ; Olafsson and Holmlid 2016). Especially the superfluidity and the Meissner effect at room temperature and at a few hundred K above that are worth mentioning, since this is the first material found with super properties above room temperature (Andersson and Holmlid 2011; Andersson, Holmlid and Fuelling 2012; Holmlid and Fuelling 2015). The most useful formation process for ultradense hydrogen employs chemical catalysis, and one of the main fields of application is within particle physics. Other applications are within space physics (Holmlid 2018b) , nuclear fusion (Holmlid 2017d,e), hydrogen storage and material characterization . The main theme may be considered to be in the field of cluster science but then in a very specialized range due to the extremely small physical size of the clusters studied: a 30-atom H(0) cluster normally has a size less than an ordinary hydrogen atom bond, and the resolution in the bond lengths measured is in the femtometer range. Most of this research has been done by researchers at Gothenburg University, Sweden. It has been replicated and verified by researchers in Norway and Iceland. This research field is of great interest for future energy development in the world and a separate research project was initiated in Norway in 2015 to verify some of the results presented in this paper.The research group in Norway has built several H(0) reactors and have since 2016 detected and verified relativistic meson velocities <0,7c from ultra-dense deuterium, distance dependent meson decay from ultra-dense hydrogen clusters, muon spectra

in PMTs, electricity from charged particles moving through coils, neutron detection from muon capture and muon catalyzed fusion, detection of multiparticle emission from hydrogen H(0) clusters, X-ray and microwave elimination studies.

A third research group from Iceland started construction of H(0) reactors in 2018 and they have in January 2019 replicated and verified relativistic velocities of 0.3c-0.9c from ultra-dense hydrogen. The present review paper is designed to connect the different subfields and to provide a guide for further research in this scientifically central field concerned with the forms of matter at the three different length scales.

The wider context of this review is the fundamental forms of matter at the three different length scales according to Hirsch (2012). The relation of these length scales through the fine structure constant α is extremely interesting, and ultra-dense hydrogen and ordinary Rydberg matter of hydrogen are the two smallest length scales with the superfluid and superconductive form at the largest length scale. *Thus, these condensed forms of hydrogen contain the physics of all the three different length scales of matter which has not been understood previously*. The famous "zitterbewegung" of the electrons due to Schrödinger gives clearly observable physical effects in ultra-dense hydrogen. The short interatomic distances in ultra-dense hydrogen , measured with femtometer resolution, gives a new background to the facile nuclear processes observed both spontaneously and after laser-pulse induction. This is a new (or revived) context for nuclear physics which does not require large experimental facilities. It however requires other experimental facilities as explored here to fully understand the fundamental physics involved. The survival of mankind may depend on how well and fast this small-scale nuclear physics in ultra-dense hydrogen can be implemented for energy production on Earth and for space propulsion. In the time of "nanomaterials", it should be

noted that ultra-dense hydrogen is indeed a picomaterial, probably the only possible picomaterial.

1.1. Relation to other forms of matter

Chemists nowadays normally occupy themselves with molecules formed by covalent bonding, since living organisms are often built from such compounds. Of course, ionic compounds like different salts are still very important for example for pharmaceutical drugs, and hydrogen bonding is important within or between large molecules for example in living organisms. But somewhere on the road into such important applications of chemical bonding and structure some fundamental points have been forgotten and left over to physicists, firstly the idea that the electrons will shield the atomic nuclei from repelling each other and that this is the general principle of forming chemical bonds and compounds. Secondly, the principle that the electrons need to be in states specified by a few well defined quantum numbers has been modified to make it possible to calculate electronic energy states with enough precision in quantum chemistry. Of these quantum numbers, the most important one is the orbital angular momentum quantum number l. The reason for its importance is the coupling of l to optical transitions which must fulfill selection rules for the transitions between specific states in the molecules due to the exact spin of $J = 1$ of a photon absorbed or emitted in one-photon processes.

So, while the electrons in covalent bonds normally have small l quantum numbers, for example $l = 0$ in a σ bond, the possibility of bonding with large l was forgotten until the idea of CES (condensed excited states) was put forth by Manykin et al. around 1980 (Manykin, Ozhovan and Poluéktov 1980,1981, 1983) , as a model for a collective excitation in a metal vapour. From that idea, it was relatively straight-forward to formulate a more general condensed state of matter called Rydberg matter (RM) with high-l bonding electrons which

shield the ions from repelling each other due to their coherent circular motion (Holmlid 1998a). *l* values up to 40-80 have been observed spectroscopically since then in RM (Holmlid 2004). A review of RM clusters exists (Holmlid 2012b).

It is always important to check the asymptotes of a model. Rydberg Matter is a metal with $l > 0$ for its conduction electrons. Very high values of *l* are easily accommodated in the RM model since atomic Rydberg states are detected with *n* up to 1000 (Sorochenko 1990). At the other end of the scale, $l = 1$ was observed to exist in RM built from hydrogen atoms (Badiei and Holmlid 2004, 2006). However, the possibility of $l = 0$ in RM was discarded for (at least at that time) obvious reasons, since a coherent motion of several electrons with no orbital angular momentum implied a contradiction. However, as realized after quite some time the spin motion of the electrons contains just the needed extra angular momentum. Thus ultra-dense hydrogen is the extreme form of Rydberg Matter with $l = 0$. IN H(0), the electron spin gives a 'zitterbewegung' or a spiraling motion with defined angular momentum, as suggested already by Schrödinger (Schrödinger 1930, Hirsch 2012, Hestenes 1990).

1.2. Detection of RM and ultradense hydrogen

RM (Rydberg Matter) was first observed here in Göteborg as a result of our intense studies of alkali metal plasmas at carbon (graphite) surfaces. These experiments were aimed at developing high-efficiency thermionic energy converters (Svensson and Holmlid 1992; Yarygin 2012) by using the formation of Rydberg states of the alkali atoms formed at graphite surfaces (Holmlid (1998b). Several doctoral students in the group were engaged in these studies, and the connection of our experimental results which gave surface work functions lower than 0.7 eV (Svensson, Holmlid and Lundgren, 1991) to the CES model by Manykin et al. was not obvious. It was Jan B.C. Pettersson, at that time a doctoral student in the group, who managed to identify this possible connection (Åman, Pettersson and Holmlid 1990).

Several types of new experiments (Åman et al. (1992); Engvall and Holmlid, 1992; Olsson, Svensson and Davidsson 1995) soon proved that Rydberg species and RM were indeed observed. Of special importance were the more complex experiments initiated soon with laser-induced TOF-MS (Wang and Holmlid (1998, 2002) ; Badiei and Holmlid (2002a, 2002b)). Some methodological observations from this early work are collected in a popular science article in the Swedish language (Holmlid 2003). Doctoral student Shahriar Badiei who was mentioned in that article mainly studied H(1) and higher H(RM) levels (Badiei and Holmlid 2004, 2006). Towards the end of his Ph.D. period, we observed even faster thus more energetic TOF-MS peaks than those from H(1), which could have been x-ray artifacts due to the laser pulse. Badiei did not have time to investigate these peaks before leaving after his PhD exam, but LH started on that work as soon as possible. This resulted in several publications using the TOF-MS method on H(0) (Badiei, Andersson, and Holmlid 2009, 2010a, 2010b) which finally proved the existence of H(0). For some time initially this form of matter was believed to be an inverted Rydberg Matter called H(-1) (Holmlid 2013a, 2013b, 2014) since $l = 0$ still appeared to be impossible. "Inverted" here implies that the roles of electrons and nuclei were thought to be interchanged due to the interaction between the electrons which gave them a very large effectivee mass. However, further experiments and also theoretical investigations into the (quite impossible) structure of H(-1) made it clear that H(0) was indeed observed (Holmlid and Fuelling 2015). The theory of three different length scales in matter for example given by Hirsch (2012) was of crucial importance for the final description of H(0) as closely related to RM H(l). The relation of these different length scales through the fine structure constant α is illuminating and extremely interesting, and ultra-dense hydrogen and ordinary Rydberg matter of hydrogen are the smallest two length scales with the superfluid and superconductive form of H(0) at the largest length scale. *Thus, these condensed forms of hydrogen H(0) contain the physics of all the three different length scales*

of matter which has not been understood previously. This is the fundamental physics of matter which seems to have been overlooked for decades. The direct coupling to nuclear processes with meson formation at low energy as described below indicates that a better understanding also of the quark structure of matter might be reached by further studies of ultra-dense hydrogen.

2. Proving the ultra-high density of H(0)

A classical method that is often used to measure distances in crystals and molecules is x-ray diffraction. This method normally requires wavelengths of the order of the distances to be measured. In the present case with internuclear distances of around 1 pm and less, this corresponds to 1.2 MeV gamma radiation. While such a method may not be impossible to use in the future if suitable equipment can be found, a few laser-based small-scale methods (described below) have been developed instead, and they are much better suited to the explorative research needed at the outset of this new field of research. Like most advanced experimental methods, the laser-induced cluster fragmentation TOF-MS method originates a long way back in the history of science, and it is not possible to here give more than a quick sketch of what science this method is based upon, especially concerning the CE process. However, the second type of experiment described here has a widely known background in the field of optical rotational spectroscopy of molecules. The third method proving the short distances in ultra-dense hydrogen which is based on nuclear reactions is however unique with no similar experiments performed on any type of system by any other group. Thus, it has to be understood from the published studies using this method. The meson showers generated are similar to those from baryon annihilation processes (Klempt, Batty, & Richard, 2005). After more than a century of nuclear physics it seems that the underlying force acting in the nucleus remains a puzzle and that the Coulomb force is the only acknowledged electromagnetic

interaction in a nucleus (Cook 2010) . Thus, nuclear processes in general and thus also the nuclear processes involved in the present experiments are not yet well understood.

One argument against the very short interatomic distances in the pm range in H(0) often put forward is the following: it is thought that the repulsion between the electrons and/or the nuclei will become so large that such short interatomic distances cannot be reached. The Coulomb interaction energy terms all have the form

$$W = \frac{\pm e}{4\pi r \varepsilon_0} \quad (1)$$

where ε_0 is the vacuum permittivity, e the unit charge on the particles (electrons and ions) and W the energy for the interaction between the two charges with equal charge signs (plus sign) or different charge signs (minus sign). See Fig. 1. Such an argument means of course that the basic physics is incorrectly understood by the person presenting the argument above about the repulsion and the situation is explained already in Holmlid (2013a), and in the same way in Holmlid and Olafsson (2016): "A pair D–D or p–p contains two electrons and two ions. No inner electrons of course exist for hydrogen, and thus the ions are bare protons or deuterons, of very small size relative to the pm sized inter-particle distances. The pair-wise interactions between the four particles, with the interaction distances of similar size, are two repulsive terms (++ and −−) and four attractive terms (+−).Thus, such a pair increases its stability with shorter distance scale as 1/r. At typical inter-particle distance of 2.3 pm, the total electrostatic energy is of the order of -1 keV thus a bound state. With different spin states for the two electrons, they may fill the same space and one of the repulsive terms (−−) disappears effectively. Thus, the stability of a pair of atoms in the ultra-dense form is increased by different electron spin states." If such a pairing of the spins indeed exists in the common spin states of H(0) is not yet known, but the argument about the strong bonding at short distances is correct anyway. See Fig. 1.

It is obvious that it is the existence of well-defined angular momentum quantum states that makes the ultra-dense hydrogen stable. The same is of course true also for ordinary Rydberg matter (Holmlid 2012b). It took about 70 years from the acceptance of quantized angular momentum in atoms, until the observation of Rydberg matter formed by such quantization was first reported in 1990-91 (Åman, Pettersson and Holmlid 1990; Svensson, Holmlid and Lundgren 1991); certainly, the special form of Rydberg matter called condensed excited states (CES) was predicted by Manykin et al. on theoretical grounds around 1980 (Manykin, Ozhovan and Poluéktov 1980,1981, 1983). It took further almost 30 years before ultra-dense hydrogen was reported in 2009 (Badiei, Andersson and Holmlid 2009), indeed without any theoretical prediction. It is remarkable that such a long time was required to realize the simple fundamental theoretical rules governing matter, namely that angular momentum quantization is the dominating effect and that energy quantization follows from this. Of course, this conclusion is easier to draw from atoms or from Rydberg Matter than from molecules containing mainly covalent bonds, where vibrational energy often dominates.

2.1. Coulomb explosions

A Coulomb explosion (CE) is the fast break-up of a molecule or cluster when the bonding forces in the entity cannot hold it together against the Coulombic repulsion forces between an excess of charges of one sign, most commonly due to repulsion between positive ions when a few bonding electrons have been removed for example by a laser pulse. This repulsion gives an initial energy to the fragments, called kinetic energy release (KER), which depends on the distance between the positive charges at the instance of electron removal. CE measurements give the distances between the positive charges in the ultradense H(0) material with the laser in operation, thus with the H(0) clusters in the radiation field from the laser. This radiation

field is quite weak, with the laser most often used in our experiments here being a < 0.5 J Q-switched laser with pulse length in the 5 ns range. Thus, ponderomotive forces (Silfvast 2008; Hora 2000) are small and will have no importance for the distances observed. The reason why such a weak laser can be used to create CE in very strongly bound clusters H(0) is that its interaction is mainly with the highly excited superconductive electrons in H(0) (Holmlid 2013a, b) which are excited or ejected by the laser pulse. Another factor for the success of this method is that the bonding in RM is only due to the conduction electrons which are removed by the laser pulse. When CE experiments are performed on ordinary molecules, the KER is lower than the repulsion energy, since some energy is used up to break still existing covalent bonds in the molecules. (Zewail 2000).

The most easily understood measurements are time-of-flight (TOF) experiments initiated by the laser pulse, with no voltage attached to the laser target where the H(0) material is located, and thus without "external field" acceleration of any ions formed at the laser target. This means that only the energy released by the CE process (KER) gives the kinetic energy of the ionic or neutralized fragments. Since no accelerating field exists in the apparatus during this kind of experiment, the TOF is the same for ionic and neutral fragments if they have the same initial velocity (kinetic energy). (Alternatively, a voltage can be applied to the laser target supporting the H(0), to directly observe which TOF peaks are due to neutrals, since they do not change their TOF with the applied voltage). Two typical TOF spectra from the same experiment using D(0) are shown in Fig. 2. The reason why the clusters or atoms move with a kinetic energy of several hundred eV is the CE process, since no voltage accelerates the particles: no such large kinetic energy can be found for any particles from laser interaction with ordinary molecules or clusters. The shortest TOF should be found for the lightest fragment, and since deuterium is used in this experiment the smallest fragment mass is 2 u.

This gives an energy of 630 eV for the neutral or ionic fragment with mass 2 u at 400 ns TOF with 101 mm distance to the detector. The fraction of the total kinetic energy release (KER) that is observed on each fragment depends on the mass ratio of the two fragments. If this 630 eV is on a light fragment ejected from a heavy cluster, the total KER is close to 630 eV. If this D fragment is one of two D ↔ D fragments, the total KER is 1260 eV. If H atoms would be formed by nuclear fusion D+D and they would give the dominating signal in the experiments, the KER would be 315 eV for one light fragment with mass 1 u, or 630 eV if two equal H fragments were formed. The Coulomb energy formula gives for the total kinetic energy KER equal to E_{kin}

$$r = \frac{1}{4\pi\varepsilon_0}\frac{e^2}{E_{kin}} \qquad (2)$$

where ε_0 is the vacuum permittivity, e the unit charge on the fragments and E_{kin} the sum kinetic energy for the fragments (KER) from the CE. E_{kin} equal to 630 eV gives 2.3 pm, 1260 gives 1.15 pm, and 315 eV gives 4.6 pm. By extensive measurements with both H(0) and D(0), and with applied voltages to give TOF-MS spectra with variable acceleration voltage (Badiei , Andersson and Holmlid 2009, 2010a; Andersson, Lönn and Holmlid 2011; Andersson and Holmlid 2012a, 2012b), it is concluded that the results in Fig. 2 for D(0) correspond to 630 eV on one D fragment ejected from a larger cluster and thus 2.3 pm D-D distance, in this case for spin value s=2. This is convincing evidence for the short distances in H(0): the results for other spin values s = 1 and 3 (Holmlid 2013a,b) support this description. The other TOF peaks in Fig. 2 are assigned as shown in the figure.

In many TOF-MS experiments also two different flight lengths to the detectors (101 and 1120 mm respectively) have been used simultaneously. This advanced construction is shown schematically in Fig. 3. The construction of the detector at short flight length is shown in Fig. 4. The catcher or converter foil gives a better detection of fast neutrals. Together with

variations of the accelerating voltage, this means that a large number of internal checks are possible in the experiments. In such experiments, the energy given to neutrals is only due to the initial KER in the laser-induced fragmentation of the H(0) clusters. The energy given to the ions is the contribution from the KER plus the acceleration (or deceleration) energy provided by the electric potential between the emitter and the grounded entrance slit of the TOF spectrometer. These two contributions can be observed directly in reduced plots like the one in Fig. 5. There, the time scale for each TOF-MS spectrum is recalculated by the multiplicative factor $(U/U_{\max})^{½}$ where U_{max} is the maximum accelerating voltage used in the experiment. In this way, the differences in TOF (in the flight path after acceleration with U V) are compensated for and all mass peaks with just acceleration in the electric field (thus without KER) should be located vertically above each other in the spectra (Holmlid 2011a). Thus, any tendency for a peak to move towards shorter reduced TOF at lower accelerating voltage directly indicates a KER process giving excess energy to an ion or a neutral particle (Holmlid 2013a, b). In Fig. 5, the large KER given to large cluster fragments is easily observed, while the small H_2 fragments have a slightly smaller KER and are more constant on the time-scale in the plots: this means that they are ions H_2^+ and are accelerated by the electric field. The H_2 TOF with zero target voltage is around 8 μs, thus a kinetic energy from the CE process of approximately 200 eV.

The problem of measuring the interatomic distances in both ordinary RM and in ultra-dense hydrogen H(0) has been solved by measuring the time-of-flight (TOF) of the fragments ejected by laser-induced Coulomb explosions and then using Eq. (2) above to find the distances. This approach is quite simple and straight-forward.

2.2. Rotational spectra

In several CE experiments described above, a rotational energy transfer during the laser-initiated ejection of the fragments of chain clusters $H_{2N}(0)$ from a surface was observed (Andersson and Holmlid 2012a; Holmlid 2013a,b). This was thought to indicate that rotational effects could be observable in $H_{2N}(0)$ clusters also in the gas phase, possibly by spectroscopic methods. Such spectral features turn out to be observable (Holmlid 2017a, 2018a) with laser excitation in the $H_{2N}(0)$ containing gas. The normal photo-multiplier (PMT) detectors used in optical spectroscopy are most sensitive in visible light and much less in the infrared. This means that the spectra observed by ordinary visible spectrometers do not cover the lowest rotational quantum numbers with spin quantum numbers $s = 1$ and 2 in H(0), but mainly cover higher values $s = 3$ and 4. Anyway, numerous rotational emission peaks which agree well with the predictions for two-atomic groups with very short distances in chain clusters $H_{2N}(0)$ can be studied. The so far published spectra (Holmlid 2017a, 2018a) agree well with p-p, D-D and p-D pairs in the chain clusters, for small rotational quantum numbers J and spin numbers $s = 2$, 3 and 4. The precision of the bond lengths is quite good, with error limits of the order of 0.1% or 0.003 pm, thus as small as 3 fm. For example $J = 1 \rightarrow 0$ with $s = 3$ gives a D-D distance of (5.052 ± 0.003) pm. For $s = 2$, the D-D distance is 2.23 pm, close to the theoretically found value of 2.240 pm (see below) (Holmlid 2013a). A recalculation from the best value 5.052 pm for $s = 3$ gives (2.245 ± 0.002) pm for $s = 2$. Two other rotational transition lines are shown in Fig. 6. The shape of the lines differs from atomic emission lines. The dimensional factor for the two lines shown differs by only 0.2%, which could be due to differences in the position of the D-D pairs in the clusters, for example at the end or inside the cluster. Due to the high temperature during these experiments, the clusters are probably relatively short, just having a few D-D pairs. This may be the reason why two

lines are observed close to the nominal value 479.6 nm. The rotational transitions observed so far are summarized in Table 1.

2.3. Nuclear reactions

The third method to prove the ultra-high density of the H(0) material is different from the two previous, in that it not only observes the material after interaction with the laser beam, but also without any laser interaction. This method builds on the immediate understanding that interatomic distances less than 1 pm will lead to spontaneous nuclear processes. Such distances are expected and indeed observed by CE and TOF (Andersson and Holmlid 2010; Holmlid 2013a,b, 2014; Holmlid and Fuelling 2015) for $s = 1$. Any detection of nuclear processes will prove that the internuclear distances are in the low pm range.

The most clear-cut observations of nuclear processes in H(0) may be due to laser pulse impact. Fast particles in the MeV range (at particle velocities $v > 0.6c$) are ejected from the laser target covered with H(0), and they are much faster than the particles studied in the TOF and TOF-MS experiments described above. In fact, the TOF is in the few ns range even for detectors placed at 1-2 m distance, which means that PMT detectors cannot be used. Most PMTs have internal electron transit times of the order of 20-50 ns, thus with no possibility to study times in the low ns range. Since the signals are very large, the particle signal can anyway be observed by direct collection (current measurement in the mA range) in real time without any further amplification. An example is given in Fig. 7 which shows the signal from a layer of D(0) on Ta metal at two collectors in the same arbitrary direction. The inner collector was rotated out of the way for the outer collector signal measurement. Please note that the signal at the outer collector is much faster than that at the inner, and that the decay times are different. (The current observed is mainly due to muon interaction with the

collectors producing an electron current which *leaves* the collector, giving a positive signal current at the collector). In Fig. 8, the same data are shown on energy per mass unit and velocity scales. The not perfect matching at high energy (short times) is most likely due to the finite width of the laser pulse. The energy and velocity scales in the two simultaneous experiments to the inner and outer collector do not agree, which indicates that different precursor particles are observed at the two different distances (the different decay rates observed at the two collectors give the same conclusion). The particle velocities extend up to 0.5 *c*. Added magnetic fields give no effect and thus these particles are not electrons or positrons which would be deflected quite easily by the magnetic fields. Combined experiments with both magnetic field deflection and TOF show particle energies above 100 MeV and particle masses below 1 u (Holmlid 2017b). Two examples of the intermediate mesons formed (charged kaon decay observed by outer collector, and charged pion decay observed by inner collector) are shown in Fig. 7. Such particles cannot be created by the laser or any other process in the experiments, but have to be generated by reaction processes in H(0) clusters by the laser interaction. Such nuclear processes require short distances between the nuclei, < 1 pm.

Further, standard particle energy measurements have identified nuclear particles that are generated spontaneously, thus without any laser interaction. Both muons and kaons have been identified by their interaction with standard scintillators (Holmlid and Olafsson 2015a; Olafsson and Holmlid 2016) and also with metal particle converters (Holmlid and Olafsson 2015b). The observed nuclear particle energies in the scintillator-PMT detectors are several MeV, in some cases (kaons) up to 70 MeV (to be published). Such particle energies require nuclear processes in H(0) forming decaying particles like kaons and pions. These processes can only take place if the internuclear distances are < 1 pm. They are identified easily in both

D(0) and p(0), thus they are not coupled to fusion but they are due to other annihilation-like nuclear processes. Thus, the third method of proving very short distances in the H(0) material is highly successful.

3. Angular momenta and distances

The short interatomic distances in H(0) are measured directly in various experiments, as already shown by three examples of methods in Section 2 above. The interpretation of these distances gives the values of angular momenta for the electrons and the quantum numbers defining the interatomic distances. First some theoretical ramifications of the angular momenta are described. One important fact about all the types of matter described here is that they are defined by angular momenta of the electrons, not by bond distances given by electrons taking part in bonds between nuclei, as is the base in most other types of chemical bonding. This also implies that vibrational motion has a minor role in the energetics of the structure. Thus this type of Rydberg matter bonding is in some senses intermediate between covalent bonding with the electrons mainly located between the nuclei in the bond, and ionic bonding, where the electrons are more or less completely transferred to one of the nuclei. In the Rydberg matter type bonding, the electrons instead spend approximately half of their time between two nuclei and thus shield the nuclear inter-repulsion. However, the most important point is that the Rydberg type bonding is similar to metallic bonding. The ordinary description of electrons in metals treat the electrons as giving longitudinal standing waves in the lattice: however an alternative description with standing waves in circular orbits (Reif 1965) is equivalent and describes Rydberg matter better.

3.1. Ordinary Rydberg matter - orbital *l*

In ordinary Rydberg matter, circular Rydberg states of atoms or molecules are combined together to form a structure which is often planar (other forms like 3D close-packing have been observed (Holmlid 2008b, 2011c). Circular Rydberg states in separate atoms are well-known in atomic physics and have the maximum angular momentum possible, with $l = n$-1 where n is the principal quantum number (Gallagher 1994). They have the longest life-times of any excited atomic states due to several well-known factors, for example the lack of overlap between the circular Rydberg state and low electronic states. In space, Rydberg states with n close to 1000 have been observed (Sorochenko 1990) and in the laboratory, at least several hundred (Haken and Wolf 2005).

Rydberg states are named after the Swedish physicist J. Rydberg, who presented the Rydberg formula (with the Rydberg constant) for optical transitions in atoms in 1888. This means that a Rydberg state is a state which is hydrogen-like (hydrogenic), thus it only involves one electron in an atom. This means that all electronic states in H atoms are Rydberg states. It is thus not correct to only associate a Rydberg state with an atomic state with large principal quantum number as is often done (Haken and Wolf 2005). It is of course true that such high-n states in all atoms are similar to Rydberg states since the single outer electron normally studied is relatively undisturbed by the inner electrons. The high n value is however not sufficient for naming the state as a Rydberg state, for example a penetrating state with large n and small l in a general atom is not hydrogenic. In Rydberg matter, the electrons are best described as being in Bohr orbits, with just one good quantum number namely l and having a classical time dependence. This means that n is replaced by l. In the lowest Bohr orbit with radius a_0, angular momentum is $l = 1$. (This is of course not the same as an ordinary s orbital

for which $l = 0$ and which description belongs to a time-independent quantum mechanical theory).

The orbital angular momentum l in ordinary Rydberg matter is not directly measured experimentally, but the interatomic distances can be measured. Since the interatomic distances are found by the CE and also in spectroscopy experiments, the relation between l and these distances must be determined. The electron orbit radius is

$$r_e = a_0 \, l^2, \tag{3}$$

since

where a_0 is the Bohr radius of 52.92 pm. This formula is valid for the Bohr model. n is not a good quantum number and it is replaced by l as described above. It is likely that the interatomic distances are so large that the electron orbits in two neighboring atoms are not in contact or overlapping, since otherwise a stable structure would not be possible. Thus the simplest approach is to determine the most stable structure of Rydberg matter. The planar shape of many clusters of ordinary Rydberg matter (Wang and Holmlid 1998; Holmlid 2007, 2008a, 2012b) makes it relatively easy to perform calculations on their stability. Electrostatic calculations of their shape and stability have been done (Holmlid 1998a). It turns out that with the assumed strong correlation between the electrons giving them a coherent motion, a stable configuration exists with planar six-fold symmetric clusters (point group D_{6h}) when the interatomic distances are 2.86 or approximately 2.9 times the radius for the orbiting electrons. This situation is shown in Fig. 9. This stable configuration was not known prior to the calculations in Holmlid (1998a). The constant 2.9 is here called the dimensional factor. Thus the result for the interatomic distances is

$$d = 2.9 \, r_e = 2.9 \, a_0 \, l^2. \tag{4}$$

The calculations for the dimensional factor only include electrostatic forces, and it is possible that magnetic effects could modify this value 2.9 somewhat. The calculations in Holmlid (1998a) were made for a 19-atom cluster, and exactly the same value of the dimensional factor was not found for 7-atom clusters. The orbital angular momentum l is the only good quantum number in Rydberg matter, possibly besides the spin (see below). Thus, in H(1) the electrons move coherently with a radius of motion of 52.92 pm.

In ordinary Rydberg matter, the cluster structure and size are determined by the orbital angular momentum of the electrons moving with l = 1, 2, 3, 4, etc (Holmlid 2012b). Due to the inner electrons for most atoms (all but H), l cannot take any arbitrarily low value. For H, l = 1 is possible since there are no inner electrons, and thus levels H(1), H(2), H(3) etc are observed Holmlid 2013a,b, , Holmlid and Fuelling 2015). The atom studied most in Rydberg matter is K, and the lowest level for K is l = 4, thus K(4), K(5), K(6), K(7), K(8) etc exist (Holmlid 2008a, 2010b), but not K(3).

The value of the dimensional factor was confirmed with high precision by rotational spectroscopy of K Rydberg matter clusters in the radiofrequency (RF) range with the number of K atoms in each cluster equal to the 6-fold symmetric numbers 19, 37, 61, 91 and with the excitation level l (earlier named n_B) between 4 and 8 (Holmlid 2007, 2008a). For the highest l values studied the dimensional factor was found to be 2.900 ± 0.005, thus with a precision of 2×10^{-3}. The average value for all types of clusters studied in the RF range was 2.865 ± 0.032, thus with a variation of 1 %. For the 19-atom clusters at l = 4, the value found was 2.8470 ± 0.0002, thus a precision of 7×10^{-5}. With a phase-delay spectroscopic method developed for the purpose of measuring general bond distances in Rydberg matter (Holmlid 2010a, 2011c), the best determination of the dimensional factor in K(RM) is 2.901 with a precision of 3×10^{-3}

at $l = 6$. This type of measurement is also sensitive to the type of material packing (planar, close-packed , FCC etc) and thus gives more information on the state of Rydberg matter formed both from K (Holmlid 2010a) and H (Holmlid 2011c). The shortest distance which could be measured ($2d$ at $l = 1$) was 282.2 ± 0.2 pm (Holmlid 2011c). These results are of great interest since they indicate that a value close to 2.9 is found also for other structures than planar, thus that there is a more general theoretical description possible which gives the dimensional factor close to 2.9 even with other cluster structures. This idea is applied to the ultradense hydrogen case below.

3.2. Ultradense hydrogen - electron spin *s*

The only state of Rydberg matter that was originally thought not to be possible was the state $l = 0$. Of course, this type of matter with $l = 0$ transcends into ordinary metal, if translational motion of the conduction electrons is possible. However, it is also conceivable that $l = 0$ can exist and that the electrons in such a case can be localized, for example forming electron pairs which are bosons and thus can be relatively closely packed. For $l = 0$, the so called 'zitterbewegung' (Hirsch 2012) is of direct interest here, with the electron spin corresponding to an orbiting motion of the electron with the velocity of light, and with the orbit radius based on the quantum electron radius $r_q = \hbar/2m_e c = 0.1931$ pm (Hirsch 2010). This definition of r_q means that the angular momentum in the orbit with this radius is $L = \hbar/2$ since the electron velocity is equal to c. This value is the half-integer spin expected for an electron. Thus, the electrons in the ultradense matter have only (or at least mainly) a spin motion and no orbital motion. How this type of motion behaves in ordinary space may, however, not be so easily visualized. For several reasons, for example the phase-delay results cited above (Holmlid 2010a, 2011c), the Rydberg matter type of circular motion of the electrons around the nuclei is still assumed to be correct for ultradense hydrogen H(0).

From the early distance measurements by CE processes in H(0), a few different distances were found. It was clear early on, that the interatomic distances were quantized, as was the case for ordinary Rydberg matter, since the same values of the distances were found repeatedly in numerous experiments. A nice picture with several different spin values s developed over a period of a few years. With the definition of the quantum electron radius r_q used here (Hirsch 2010), the half-integer spin quantum number is already included. Thus, the spin s values used here are multiples of this half-integer electron spin. Tentatively, an expression for the interatomic bond distances similar to that found for ordinary Rydberg matter was applied, of the form

$$d = 2.9\, r_q\, s^2 \quad . \qquad (5)$$

From this formula, values s = 2 and 3 were mainly observed in the CE experiments. Here, s = 2 means $L = \hbar$ or $\hbar$. The transformation (oscillation) between ordinary Rydberg matter states and ultradense states could be followed in real time (Badiei, Andersson and Holmlid 2010b).Thus it was apparent that angular momentum from the orbital motion could give higher values of the spin than what appeared to be intuitively possible for just one electron. This fit very well into the model of these types of matter as being dominated by coupled angular momenta. Later spectroscopic measurements (Holmlid 2017a) confirmed this picture of large spin values, with s values equal to 2, 3 and 4. The main conclusion is that these spins are due to electronic motion since half-integer spins are found, however other factors may add as discussed below. That the spins can be increased from $L = \hbar/2$ is a real effect even for single albeit paired electrons.

One point to observe here is that the formula for d above in Eq. (5) is not compatible with the "zitterbewegung" property that the velocity of the electron is c even for higher values of s.

The angular momentum for the electronic motion with electron velocity c is $L = m_e r_s c = s \hbar /2$ which gives $r_s = s r_q$, not $s^2 r_q$ which is the basis for Eq. (5). This means that the motion of the electrons in the ultradense hydrogen has a velocity c/s, such that the speed of light for the electron is only attained for the lowest state $s = 1$. This variation with the quantum number s is similar to that for a quantized motion in a Coulomb potential as in the Bohr model. This behavior agrees with experiments. This result indicates that the angular momentum for $s > 1$ is not a real spin, but another type of added angular momentum. Below, the vibrational motion in the H(0) structure is shown to give further angular momentum which may give the required behavior.

The interesting question is then how the electrons and nuclei (ions) are organized in the cluster structure. The basic form is clearly a pair of H atoms in a chain cluster. This shape was deduced directly from the CE cluster experiments (Andersson, Lönn and Holmlid 2011; Holmlid 2012b).The two electrons with mainly spin motion have strongly correlated motion, similar to ordinary Rydberg matter. The lowest stable state would be $s = 1$ for both coupled electrons, with the two coupled spins in the same direction since otherwise the 'zitter'-wise electron motion is not correlated. If the orbital motion in higher Rydberg matter states transfers angular momentum to the electron pair when the ultradense state is formed so that an electron circular motion will be maintained with $s > 1$, an electron pair may exist with a common spin quantum number. It is necessary that both electrons in an H-H pair have the same spin state, since otherwise the strongly correlated or coupled motion will not be possible and the cluster will not be stable. Other more complex possibilities probably exist similar to entangled states. It is thus concluded that two circling electrons exist with a common s value. In a large cluster, several such pairs are coupled together to a chain cluster, probably still with the condition that the electrons all have the same spin quantum number s.

The geometry of the chain clusters is still slightly uncertain. The assumption derived from ordinary Rydberg matter is that the two electron orbits in a H-H pair are coplanar. However, with $l = 0$ there is no planar motion of the electrons at all and the orientation of the electron motion in the "zitterbewegung" is thought to be unspecified. Thus, almost any shape of the clusters may seem possible. However, since the free rotation of the H-H pairs is observed in the rotational spectroscopy (Holmlid 2017a, 2018a), a structure with strongly interacting coplanar pairs is virtually excluded. Thus, the normally depicted cluster structure as in Fig. 10 is still the best visualization of the chain clusters.

That the same value of the dimensional factor as in ordinary Rydberg matter will apply also to the H-H pairs in ultradense hydrogen was unexpected, especially since the electronic motion is not exactly the same as in ordinary Rydberg matter. However, experimental results show that this is the case with high precision (Holmlid 2017a, 2018a). For ordinary Rydberg matter K(l), the average dimensional factor was found from rotational radiofrequency spectra to be 2.865 ± 0.032, thus a variance of only 1% (Holmlid 2008a). For ultradense hydrogen, the typical value for this constant is lower than 2.90 by only 0.2-0.5% in visible rotational spectra (Holmlid 2017a, 2018a). This indicates that a similar quantum mechanical description is valid for these different forms of matter and largely independent of distances: the experimental distance scale differs by more than 10^6 from 9.8 μm at $l = 8$ (Holmlid 2008a) to 2.23 pm at $s = 2$ (Holmlid 2017a). This extreme scale independence points to simple Coulomb forces only.

3.3. A general distance model

It is possible to combine the two formulas used for the bond distances in ordinary Rydberg matter and ultradense hydrogen into one which should be generally valid, thus

$$d = 2.9\ (a_0\ l^2 + r_q\ s^2) \qquad (6)$$

Here a_0 = 52.92 pm, the Bohr radius, while r_q = 0.1931 pm is the quantum electron radius. Their ratio is 2/α, with α the fine structure constant = 1/137.03. This implies that both effects exist in ordinary Rydberg matter, with l and s different from zero. So this formula may also be written as

$$d = 2.9\ a_0\ (l^2 + (2/\alpha)\ s^2) \quad . \qquad (7)$$

This formula shows that the contribution of the electron spins to the distances is reduced by the fine structure constant α. This is expected from a general point of view to be due to magnetic interaction between the motion of the electron in its orbit and the electron spin (Haken and Wolf 2005). However, the effect of the spin is here most obvious with l = 0, thus with no orbital magnetic dipole. Thus, thee effect of the spin is here not due to the magnetic dipole but due to the size of the electron orbit, even if the fine structure constant enters the description.

There is so far no indication that ***l*** and ***s*** couple in a spin-orbit coupling process to an angular momentum ***j***. In principle, such a process could exist. Further, there is no indication that the quantities l^2 and s^2 should be replaced by the quantum mechanical forms $l(l+1)$ and $s(s+1)$. Such an effect should be easily observed at the low values of the quantum numbers of interest for hydrogen, both for H(1) and H(0). Thus, the model used here is basically a classical description with added electronic features like electron correlation and a rotational motion to describe the spin states. It is assumed that a quantum mechanical description of several strongly interacting and coupled Rydberg states is quite complex, so it is a great advantage that a semi-classical description exists with high precision in its predictions.

3.4. Vibrational angular momentum

The hydrogen nucleus in H(0) spin state $s = 1$ is surrounded by the electron at $l = 0$, thus in a spatial distribution with its maximum on the nucleus. As is the case with any *s* orbital electron, angular momentum $l = 0$ means that the electron passes back and forth through the nucleus in straight lines. The spin quantum number $s = 1$ indicates that the electron anyway moves with the speed of light in an orbit giving the spin and the magnetic dipole of the electron ("zitterbewegung"). When $s = 2$ and above, there apparently exists an added angular momentum for the electronic motion relative to the nucleus. The simplest way to understand this type of angular momentum is to assign it to the vibrational motion of the nucleus within the Coulomb potential from the surrounding electron. Since this type of potential is spherically symmetric, two or three perpendicular vibrations in arbitrary directions describe the vibrational motion of the nucleus. This gives in general a motion with a rotational angular momentum. This is a well-known effect in molecular dynamics with important implications in molecular spectroscopy (Hollas 2004). The electrons in a cluster may be considered to be fixed relative to each other by their mutual correlation interactions and thus to give the external structure of H(0), while the nuclei vibrate inside. However, this vibrational-rotational motion will distort the spatial distributions of the electrons in $l = 0$. Moving the point of the viewer to the nucleus means that the spatial electronic distribution is displaced out from the initial position of the nucleus and this electronic distribution rotates around the nucleus due to the orbiting rotation of the nucleus. This is a special situation which is not fully described in this simple way, but this mechanism is proposed to be the reason for the apparent added spin in the higher *s* states. Thus $s > 1$ is not a real electron spin as already pointed out above. From this picture, it should also be possible to better understand the angular momentum coupling processes during the transformation between H(0) and H(1).

In the rotational spectroscopy measurements on H(0), the linewidth is relatively large, close to 20 cm^{-1} (Holmlid 2017a). This may be due to vibrational features and also due to heating of the material H(0) by nuclear processes. As pointed out in Ref. (Holmlid 2017a), the rotational transitions (observed in the rotational spectroscopy) of the rotors D_2 in the D(0) clusters may also be promoted by coupling to vibrational motion. This is of course even more likely if the vibrational motion is directly coupled to rotation as described here.

3.5. Differences p(0) vs. D(0)

There exists one clear difference in the cluster forms for protium p(0) and deuterium D(0). This concerns the distances observed in the CE experiments (Badiei, Andersson and Holmlid 2009). The CE experiments on D(0) clusters give distances of approximately 2.3 pm (s = 2) and 0.56 pm (s = 1) (Holmlid 2013a), while those for p(0) give distances of 2.3 pm (s = 2) and 5.0 pm (s = 3) (Badiei, Andersson and Holmlid 2009). Another intermediate distance was also for some time believed to exist in p(0), namely 3.7 pm (Badiei, Andersson and Holmlid 2009, 2010a). This distance is not easily described as $d = 2.9\ r_q\ s^2$ (giving s = 2.6) or $d = 2.9\ r_q\ s$ (giving s = 6.6) (assuming a linear variation with s). Not even a description as $d = 2.9\ r_q\ s(s+1)$ gives a very useful interpretation (10% error relative to 2×3). In Badiei, Andersson and Holmlid (2009), this was finally concluded to be due to the fragmentation of a p_3 group at the end of a long chain cluster, where p_2 is a separate unit due to pairing of the proton spins giving a boson in the p(0) structure. With the spin state s = 3, this gives a CE distance p - p_2 close to 3.7 pm. More details are given in Holmlid (2013b). It is also interesting to note that the normal spin s values found in CE experiments are generally higher for p(0) than for D(0), thus the average distances in the clusters are larger for protium than for deuterium. This agrees with the notion that the proton-proton (fermion) interaction should give larger bond distances in p(0) than in D(0).

3.6. Stable clusters versus plasma

The assumed impossibility of forming the small distances observed, around 1 pm, in a material is sometimes discussed. One argument put forward against such small distances is that the electron kinetic energy will become very high when the electronic motion is constrained to short distances. This argument appears to be based on the uncertainty relation $\Delta x\, \Delta p_x \geq \hbar/2$. It appears to often be used in plasma physics in this form, and should be applicable to unbound systems. From the experimental results giving very precise and repeatable measurements of the internuclear distances and well-defined quantum numbers, it is apparent that the clusters are in well-defined angular momentum and probably also energy eigen-states. Also, the line-widths in the rotational spectroscopy measurements are quite narrow. With stable clusters (molecules) the applicable uncertainty relation is $\Delta E\, \Delta t \geq \hbar/2$. Assuming first that Δt = 5 ns, thus that the state observed only exists during the laser pulse, gives $\Delta E \geq 7\times10^{-8}$ eV. This is very small relative to the bonding energies of a few keV. It corresponds to 5×10^{-4} cm^{-1}, much smaller than the spectroscopic resolution obtained. The material H(0) can exist for days to weeks in a stable vacuum environment. Thus, instead assuming Δt = 1 s gives $\Delta E \geq 3\times10^{-16}$ eV which corresponds to a frequency of 0.2 Hz or 5×10^{-12} cm^{-1}. This is much smaller than any resolution in the experiments. Thus the uncertainty relation is not in conflict with the experimental results of internuclear distances of a few pm with error limits of a few fm. With a plasma instead of clusters (molecules), the situation is certainly different also since the electrons are not distinguishable and do not have specific angular momentum quantum numbers. In the case of a bound system with clusters or molecules, the distances found are clearly compatible with theory.

3.7. Compton-scale complexes

For completeness, small atomic complexes proposed in the literature will be compared with the H(0) description. The closest resemblance is due to Mayer and Reitz from 2012 and onwards Mayer and Reitz 2012,2014). They propose a negative complex (tresino) as e-p-e with an electron-proton radius of 0.6 pm, quite close to the H(0) radius in $s = 1$ given here as 0.57 pm. They present quantum mechanical calculations which give a deep energy minimum for the tresino. Also a non-planar neutral e-p-p-e complex is proposed (quatrino). They stress the necessity of strongly correlated electrons (as implied both for ordinary Rydberg matter H(*l*) and for ultra-dense hydrogen H(0) here) to make the systems stable. They do not propose any specific quantum numbers for the electron motion in the complexes. Their description of the p_2 complexes is rather similar to the pairs in the H(0) description, but electron spins, excited states and good quantum numbers are missing. Larger clusters are not contained within the tresino description. Thus, the molecular-cluster approach used here which of course is necessary to understand H(0) was not used by these authors.

4. Formation mechanism of H(0)

The mechanism of formation of H(0) is closely related to that of ordinary Rydberg matter (RM). Several studies exist on the catalytic processes which lead to formation of ordinary Rydberg matter of potassium K (Pettersson, Holmlid and Möller 1989; Wang, Engvall and Holmlid 1999; Engvall, Kotarba and Holmlid 1999). The main process is that K atoms on a surface desorb thermally as a mixture of states including Rydberg species, not only as believed "classically" for example by Langmuir et al. as ground state atoms K and ions K^+ (Taylor and Langmuir 1933; Kaminsky 1965). This type of complex Rydberg desorption process is more probable on a non-metallic surface (Holmlid 1998b). However, the desorption process is further complicated by RM cluster formation processes in the layer just outside the

surface, of course still inside the point of no return for the desorbing atoms and ions at a certain distance outside the physical surface. These RM cluster formation processes give a much lower desorption energy for the atoms or ions included as part of a RM cluster, since the atom bonding to the surface is weakened and the bonding between the atoms in the cluster takes over and engages the valence electrons in the atoms. This process has been investigated directly by looking for the desorbing clusters after attachment of K atoms from an atomic beam to the clusters at the surface: special asymmetric multi-peaked angular distributions were found (Wang, Engvall and Holmlid 1999) as shown in Fig. 11. This type of experiment proves directly that the K_N Rydberg matter clusters are formed in thermal desorption from the catalyst surfaces.

In the same way, also Rydberg matter clusters of H can be formed, probably often by energy transfer from the K Rydberg atomic species and the K_N Rydberg matter clusters (similar to energy pooling processes proved by Kotarba and Holmlid 2009). The catalysts which are best suited for Rydberg matter and ultra-dense hydrogen formation are so called hydrogen transfer catalysts, which dissociate the H_2 molecules to separate H atoms on the surface, as also metals like Pt and Ir do. This means that the H atoms behave as alkali metal atoms on the surface and in the desorption process. Thus H_N Rydberg matter clusters form in desorption in the same way as the alkali metal clusters do. This supports the common notion that H is the lightest alkali metal (Holmlid 2010b). The Rydberg matter clusters of H designed H(l) can have l = 1, 2, 3.... and they are observed directly by CE experiments (Badiei and Holmlid 2006; Badiei, Andersson and Holmlid 2010a).

One important property of the catalyst used is that it dissociates the H_2 molecules to separate H atoms. In this way, the electrons on the H atoms are directly in Rydberg states (hydrogenic

states). If a covalent H_2 bond is formed, H(*l*) RM cannot be formed, but H_2(*l*) RM is still possible (Wang and Holmlid 2000, 2002). Also N_2(*l*) RM has been studied under similar conditions (Badiei and Holmlid 2002a), which is apparently due to the strong bond in N_2.

Ultradense hydrogen H(0) is formed spontaneously from H(*l*), probably mostly from H(1). This inter-conversion reaction can be observed in real time in CE experiments (Badiei, Andersson and Holmlid 2010b). A diagram of the relations between the different forms of hydrogen is shown in Fig. 12 similar to that in Holmlid (2014). The inter-conversion between H(1) and H(0) is indicated with (blue) arrows. The cluster structure is different in H(0), mainly in the form H_{2N}(0), than in H(1), which mainly forms planar 6-fold symmetric clusters. In the CE experiments, a memory effect can be observed in the cluster shapes (Holmlid 2012a). This effect can be seen in Fig. 13, where the processes change in time from D and D_4 ejection from large clusters with 630 eV and 9.4 eV energy respectively, to cleavage of small clusters giving fragments at 315 eV ($D \leftrightarrow D$ and finally $D_4 \leftrightarrow D_4$) and 4.7 eV respectively.

H(0) is easily deposited on a metal surface, but since it is superfluid over large temperature ranges, it is not easily collected or assembled. Instead, it creeps rapidly as a film over metal surfaces (Andersson and Holmlid 2011) like superfluid liquid helium does. That H(0) is superfluid also means that its internal rotations in the clusters are free and not hindered by the surrounding H(0) phase. This is similar to the free and undisturbed rotations of molecules inside superfluid He clusters (Fröchtenicht, Toennies, Vilesov,1994; Goyal , Schutt , and Scoles 1994). In Fig. 12, the inter-conversion from H(1) to H(0) ends up in high rotational states which do not lose their energy rapidly due to this unhindered rotation. This means that the system can oscillate back and forth between H(0) and H(1), as observed directly in real time by the CE experiments (Badiei, Andersson and Holmlid 2010b).

The chemical function and structure properties of the so called styrene catalysts used to form H(*l*) and then H(0) spontaneously has been studied by many groups during many decades. Especially the studies by Ertl and coworkers (for example Muhler, Schlögl, and Ertl 1992) have given firm evidence of their normal catalytic function. Their function to form H(*l*) and H(0) has not been studied, since the catalysis workers never looked for such features and certainly lacked methods to detect H(0). The studies of the intriguing aspect of formation of Rydberg species at such catalysts, on which the formation of H(*l*) and H(0) relies, has been initiated here in Göteborg (Holmlid et al. 1993) and studied further in the catalysis group in Cracow, lead previously by A. Baranski and later by A. Kotarba. A fruitful cooperation in this field has existed for 25 years between our groups, initially catalyzed by Govind Menon (Holmlid and Menon 2001). The present review is intended for a general physics audience, and thus much detail on the complex science of the catalysts used is not included here. Such a fuller treatment is better suited for the catalytic literature. Only a few recent common publications are mentioned here as examples of the unique methods used and as evidence of the detailed information that can be found by these methods, Stelmachowski et al. (2015), and Trebala et al. (2011). Kotarba et. al. (2000) is further a central publication on the function of these iron oxide catalysts.

The formation of Rydberg states of the K promoter on catalyst surfaces was studied early by Engvall et al. (1994) and Kotarba et al. (1995). Rydberg state formation on carbon surfaces was studied with angular resolution (by Andersson, Wang and Holmlid 1996) and using very fast desorption methods by Holmlid (1998b). This fast desorption study Holmlid (1998b) gave an unprecedented insight into the desorption of Rydberg alkali atoms from solid surfaces. Holmlid (1998c) showed Rydberg desorption also from a metal oxide surface. The

direct proof of desorption of Rydberg atoms from solid surfaces was however given much earlier (Pettersson and Holmlid 1989; Engvall and Holmlid 1992). Several later studies also identified alkali Rydberg species at important catalyst surfaces (Engvall, Kotarba, Holmlid 1994, 1999; Andersson, Wang and Holmlid 1996; Kotarba et al. 1995).

4.1. Stability of H(0)

Speculations about a low stability of H(0) are of course completely meaningless. Due to the bond energies close to 500 eV (see section 2 above), this is the most stable form of condensed matter that exists in the Universe. H(0) is stable at temperatures at least up to 1 MK (Holmlid 2018b) and thus it exists even in most stars. It is likely that this was the primordial form of hydrogen in the Universe before star formation started. In experiments at low pressure, it exists virtually unchanged for days and weeks as shown by the TOF and TOF-MS spectra from the first single-shot laser pulse. The spontaneous nuclear processes in H(0) can be monitored for weeks. These processes are stimulated somewhat by light from fluorescent tubes in the laboratory, so covering the windows in the apparatus is useful for keeping the H(0) stable for long times.

5. Cluster shapes in H(0)

5.1. Chain clusters

The structure of H(0) clusters as composed of H-H pairs forming a chain $H_{2N}(0)$ was established early on by the analysis of the TOF and TOF-MS spectra from CE experiments (Andersson, Lönn and Holmlid 2011; Andersson and Holmlid 2011) using unsupported H(0). It was concluded that the clusters observed after ejection of small fragments were H_8, H_{10}, H_{12} etc (Andersson, Lönn and Holmlid 2011). It was also found that the clusters were often split in the middle, forming fragments with half the KER thus 315 eV in state $s = 2$ (Andersson and Holmlid 2012b) as also shown in one case in Fig. 13.

The chain clusters are the ones that have super properties, like superfluidity and superconductivity. This appears to be due to the possibility of some of their electrons to be excited into more Rydberg-like orbits in the conduction band (Hirsch 2010,2012). This effect is observed directly in CE experiments where the temperature of the H(0) layer on a metal is increased above a transition point, at which the chain clusters disappear (Holmlid and Kotzias 2016). In a magnetic field, the chain clusters float above the carrier surface and thus show a typical Meissner effect (Andersson, Holmlid, and Fuelling 2012; Holmlid and Fuelling 2015).

5.2. Small clusters

Small clusters of H(0) are observed mainly as $H_3(0)$ and $H_4(0)$ (Holmlid 2011b). There is no strong indication that free clusters $H_2(0)$ exist. The small $H_N(0)$ clusters have no super properties. They show no Meissner effect and they thus mainly reside on the magnet surface in such experiments (Andersson, Holmlid, and Fuelling 2012; Holmlid and Fuelling 2015), and they do not disappear at the transition temperature as the chain clusters do (Holmlid and Kotzias 2016). On the other hand, they seem to be the clusters in which nuclear processes take place, since such processes are observed on the carrier surface even above the transition temperature point where the chain clusters disappear (Holmlid 2019).

The small H(0) clusters normally give neutral fragments in the CE experiments. This is seen in Fig. 14 from a CE experiment with varying acceleration voltage, where the fast signal at around 400 ns from the small clusters is unchanged by the acceleration voltage. (Some contribution from atoms ejected from chain clusters to this peak is of course possible, as discussed further below). These fragments often have an energy of 630 eV or higher, as described in the study of the CE processes with several charges (Holmlid 2011b). In Fig. 14,

their energy per D atom is 500-1200 eV. (This high energy makes it unlikely that they are fragments from large clusters, since that would indicate state $s = 1$). Their neutrality indicates that they are D atoms, formed by attaching one electron to the D^+ ion at the target after the CE process is finished. This means that they are not so easily observed in the TOF experiments with a long flight path, since the detector used in such experiments only detects ions. This can be observed in Fig. 5. With a short flight path, a detector with a catcher foil was used as shown in Fig. 4, which also detects neutrals, as seen in Figs. 13 and 14. The reason why the small clusters do not give stable cluster ions is the bonding with few electrons in the cluster with small internuclear distances: CE indeed takes place when one electron is removed from the cluster. This gives H^+ ions primarily and H atoms after neutralization, and few small cluster ions.

The peak around 400 ns which is assigned to small clusters $D_3(0)$ and $D_4(0)$ can possibly also have contributions from fragmentation of chain clusters. There exist however several experiments where the small H(0) clusters are observed better separated from the fragments from the chain clusters, so that fragments from chain clusters can be excluded safely. The most direct experiment may be the TOF observations from CE processes, where atoms D can be observed from the process 8(4+)S in $D_4(0)$ and from the process 6(3+)S in $D_3(0)$. These processes are reported in detail in Holmlid (2011b). They give unique TOF peaks as seen in Fig. 15 (cf. also (Andersson and Holmlid 2012a). In this experiment, the temperature of the D(0) source was low as well as the laser pulse-energy to avoid large clusters and unnecessary fragmentation. In this way, fragments from the higher and thus more easily ionized $s = 3$ state dominate the detected signal at longer times, and $s = 2$ only gives signal at short times from small clusters.

Another type of CE based TOF-MS experiment studied the back-reflections of D^+ ions with a few hundred eV energy from a surface layer of $D_3(0)$ and $D_4(0)$ on the catalyst used for forming D(0) (Andersson and Holmlid 2012a). All ions D^+ formed by the CE process initially moving towards the catalyst surface were reflected with the correct energy loss from $D_3(0)$ and $D_4(0)$ clusters, giving well separated TOF-MS peaks. This result is unique especially in the respect that all ions were reflected: such a process has never been observed in ion scattering studies in other systems. This indicates that such small clusters exist at large densities in the boundary layer outside the catalyst surface, not only on the surface. Similar reflections from chain clusters do not seem possible.

In the experiments where the D+D fusion reactions were studied by TOF-MS (Olofson and Holmlid 2014b), collisions of fusion products against $D_4(0)$ clusters were detected. The colliding fusion products were ^{4}He, ^{3}He and p. Due to the high energy of a few MeV of the particles from the fusion process, fragmentation processes are indeed expected in their impact on $D_4(0)$. The processes observed included scattering of one fast D against the remaining D_3 cluster part, thus fragmentation of the D_4 clusters was observed. This type of experiment thus proves that the $D_3(0)$ clusters are strongly bound, since the D_3 clusters were not fragmented further by the impacting D nucleus.

The free clusters $H_3(0)$ and $H_4(0)$ have also been searched for in rotational spectroscopy experiments with no success (Holmlid 2018a), Certainly, groups like p_3, p_4, D_3, D_4, $(pD)_2$, pD_2 and p_2D have been detected as summarized in Table 1, but they are still rotating groups inside the chain clusters, not free clusters (molecules) rotating in 3 dimensions. However, if the internuclear distances are just slightly smaller than expected from the dimensional factor 2.90, the signatures of the free clusters (molecules) may be quite difficult to assign due to

peak overlap. Also, since the properties of the special type of spin angular momentum (due to vibrations) in this case are not well known, the rotational transitions of small free clusters may be difficult to identify.

5.3. Other cluster shapes

It may seem that the planar six-fold symmetric clusters of the ordinary Rydberg matter have very little relation to the chain clusters in ultradense hydrogen. However, there exists a form of cluster which is intermediate between these cluster forms, and that is the stacks of planar six-fold symmetric Rydberg matter clusters studied in Holmlid (2011a). This type of cluster still involves planar clusters and not only the pairs in $H_{2N}(0)$. However, the bonding between the pairs to form the chain clusters may be similar to the bonding between the K_7 clusters observed in these TOF-MS experiments. Such CE experiments however give no values of the bonding distance between planar clusters.

In the phase-delay light-scattering studies of H(*l*) (Holmlid 2011c), one distance at 1.20 - 1.34 nm was tentatively assigned to (twice) the intercluster distance *d*(2), thus for H(2). The reason for this was of course the approximate agreement with the expected distance, but also the variability of this distance in the experiments. In cluster stacks of varying size, the distance between the separate cluster planes is expected to vary somewhat due to the weak bonding between the planes in the stacks. The excitation state H(2) found in these experiments is still seldomly observed in the CE experiments, apparently due to its rapid deexcitation to H(1) (Andersson, Holmlid, and Fuelling 2012; Holmlid and Fuelling 2015). However, in a magnetic field as in these references the situation is changed.

At present there is no strong indication that dense continuous three-dimensional (3D) bodies are formed from H(0), despite the suggestion of such forms in the literature (Winterberg 2010 a,b). The attractive internal forces or cohesive forces would have to be very strong to hold such a material together in ordinary gravity, since the density is of the order of 100 kg cm^{-3}. Such cohesive forces are unlikely in the known largest structure of nm-sized chain clusters. A cloud of such clusters $H_{2N}(0)$ can be observed by CE processes in a vacuum hanging or slowly falling around an H(0) catalyst source (Andersson, Lönn and Holmlid 2011). Its varying density and cluster composition is then easily studied. Layers of H(0) are also easily observed on surfaces, even on vertical surfaces or on the backside of various objects due to the superfluid properties of H(0) at room temperature (Andersson and Holmlid 2011). However, large bodies of H(0) have not been observed directly.

One type of dense matter observation may however be close to continuous H(0). Under the conditions of interest, the vacuum chamber is filled with a visible mist, probably of H(*l*) Rydberg matter. Such a mist is formed after an hour or so of direct laser impact on catalyst pieces with the hydrogen gas pressure in the mbar range. This can be seen in Fig. 16 using D_2 gas. Note the visible cloud that scatters the white light generated by the interaction of the IR laser with D(0). It is then also possible to observe small laser-initiated particles glowing with white light for a few seconds in the deuterium atmosphere. They move with a velocity of a few m s^{-1} and can collide and bounce from surfaces inside the apparatus while glowing continuously. This can be seen in a small video attached with one frame shown in Fig. 17. It is likely that these particles consist of D(0) and that the process giving the white light is the condensation of hydrogen Rydberg matter D(*l*) onto the particle of D(0), as discussed further below.

6. Magnetic properties of H(0)

Numerous CE experiments with several different configurations of the laser beam on small permanent magnets placed in the flux from a source of p(0) (Holmlid and Fuelling 2015) and D(0) (Andersson, Holmlid and Fuelling 2012) have been done. They all show a strong variation of the TOF signals with the magnetic field strength using both short and long TOF distances, both with pulse counting (MCS) and with direct oscilloscope TOF observations. The conclusions from these studies were that the chain clusters $H_{2N}(0)$ exhibit a Meissner effect, thus that they float in the magnetic field above the magnet surface. An example of this behavior for D(0) is shown in Fig. 18 and one example for p(0) by changing the lateral distance of the laser beam to the surface in Fig. 19. In the case of p(0), it was even shown that the laser depleted the cloud of the lifted clusters much more rapidly than lower levels close to the surface. Thus, these floating clusters are not in contact with the surface or renewed from there rapidly.

A magnetic field stronger than 0.05 T prevents the formation of H(0) (Andersson, Holmlid and Fuelling 2012). Thus the formation of the chain clusters is inhibited by the magnetic field. Since these clusters possibly are involved in the formation of the small clusters $H_3(0)$ and $H_4(0)$, the density of small clusters may also decrease strongly in a magnetic field. This means that it is difficult to selectively destroy or remove only the chain clusters in a magnetic field and still be able to study the small clusters $H_3(0)$ and $H_4(0)$ in the magnetic field. In fact both the interacting cluster forms H(0) and H(1) are suppressed in a magnetic field, as shown very clearly in Fig. 20. Instead, the lowest energy Rydberg matter cluster form that can exist in the magnetic field is H(2), which is difficult to observe in other experiments probably since the material then is rapidly deexcited spontaneously to H(1) and H(0). This means that it is not absolutely clear that the small clusters $H_3(0)$ and $H_4(0)$ can exist in a strong magnetic field

where the chain clusters disappear, since the small clusters may be few when the reaction path forming them is broken. However, they exist in slightly weaker fields where they can be formed from chain clusters as shown in Fig. 18. There is no lifting of the small clusters observed either, so it is likely that they still reside on the magnet surface. Theoretical arguments certainly support this (Andersson, Holmlid and Fuelling 2012). This formation problem for small clusters is the probable reason for the different conclusions reached in Andersson, Holmlid and Fuelling (2012) and Holmlid and Fuelling (2015), concerning if the small clusters stay on the magnet surfaces. An improved conclusion on this point would require further studies with easily variable magnetic field strength using an electromagnet.

7. Surface properties of H(0) clusters

The description of the formation processes for H(0) given above could mean that the H(0) clusters which leave the catalyst surface will not be able to survive on other types of surfaces. For example, the source described in Andersson, Lönn and Holmlid (2011) may just be able to form a cloud of H(0) clusters in the gas phase and not be able to deposit clusters H(0) on any support. Results of this type are shown in Fig. 2. However, this was soon proved to be possible by letting the clusters fall down on other surfaces, where they could easily be studied using CE processes initiated by the laser (Andersson and Holmlid 2011). The H(0) clusters could even be trapped onto a vertical surface by a suitably arranged grid below the source (Holmlid 2013b) and Fig 4. This construction was based on the understanding that the H(0) material is superfluid. The structure of the cloud around the source, with mainly higher H(*l*) Rydberg matter states at a distance from the catalyst (Andersson, Lönn and Holmlid 2011), agrees well with a process where the dense H(0) clusters fall rapidly down to the support. The less dense H(*l*) clusters fall much slower and thus form the main part of the cloud.

The TOF and TOF-MS spectra using H(0) deposited on a material are often more complex than the H(0) spectra from the gas (cluster) phase. This is not unexpected, since the recoil of the two (or more) fragments from the H(0) cluster often involves scattering from the surface of the support. The geometry of the cluster on the surface may also differ a lot, for example if a chain cluster stands perpendicular to the surface, or if it lies parallel to the surface. Due to the small size of the clusters, it is even possible that H(0) clusters are deep in the recesses between two surface atoms, or that each H(0) cluster is on top of a surface atom. Further, due to the super properties of the chain clusters, their relation to the surface and especially to the electrons in the surface is not well known. Thus, several new and not well understood parameters may be involved in the specification of the state of a H(0) cluster on a surface. This field is of course novel and quite extensive, and much remains to be done on these aspects. Just a few crucial experiments have been done in this direction.

The variation of the TOF signal with laser focus position on a surface around the boundary between a metal (steel) part and a plastic surface (of three different types) was studied in one publication (Olofson and Holmlid 2012). The distance between two consecutively studied laser-spot positions was approximately 50 μm. On the metal surface, the TOF spectra were constant independent of the laser-spot position. Many new features could be observed on the plastic surfaces, for example that D(1) does not exist on hydrogenated plastic surfaces. With a fully fluorinated plastic (PTFE) surface, small D(0) clusters did not exist on the surface. It was further shown that the neutral fragments of chain-clusters of D(0) became slower, the further away from the metal-plastic boundary the laser-spot came on the plastic surface. The D(0) was replaced on the surface by D(1) at the same time. The shifting of the TOF spectra to lower kinetic energy was concluded to be due to rotational excitation during ejection for the horizontally arranged clusters at low density on the plastic surface. This is the same

mechanism which was observed in the CE TOF-MS experiments on metals with variable acceleration potential for p(0) and D(0) (Holmlid 2013a, 2013b). The process observed in these TOF experiments is easily understood dynamically, since fragmentation of a horizontal cluster on the surface can only eject the fragments from the surface after a rolling excitation of the fragments over the surface has taken place, followed by scattering off the surface (Andersson and Holmlid 2011). This type of dynamical rotational excitation process also exists in surface scattering of molecules against surfaces (Andersson, Olsson and Holmlid 1986; Pettersson, Nyman and Holmlid 1988; Nyman, Holmlid and Pettersson 1990).

Experiments have also been done of the so called "fountain effect" (Guénault 2003) expected for the superfluid H(0) layer on surfaces (Andersson and Holmlid 2011). In this case, the CE TOF spectra were studied on and above a 1 cm long steel capillary attached vertically to an open container of D(0). It was shown that D(0) existed also above the tip of the capillary, and that the transport there was relatively slow compared to the transport on the outside of the capillary. Thus, the D(0) did not move on the outside but inside the capillary as should be the case if a fountain effect exists. The transformation between D(0) and D(1) makes the situation quite complex, since D(0), moving from the superfluid phase into the cluster phase above the capillary, will convert quite rapidly to D(1). A fountain effect is verified since the interconverting states D(0) and D(1) are detected by the laser above the top of the capillary.

8. Nuclear processes in H(0)

Nuclear processes exist in H(0), both in p(0) and D(0). These processes are not only fusion processes (of course only existing in D(0)), but other types of nuclear processes in fact dominate. Both laser-induced and spontaneous processes have been studied. These processes cannot be described as fusion reactions since they do not give the products expected from

normal nuclear reactions. Instead, they much more resemble annihilation reactions from their product spectrum (Klempt, Batty, and Richard 2005). They thus seem to belong to a novel type of nuclear reaction which may be directly coupled to the transformation of quarks inside the nuclei. Such experiments have not been performed by any other research group, and it is thus not possible to give any references to other studies.

The main type of experiment used here has not only been able to observe the particles formed by the nuclear processes but has also been able to observe the particle decays directly (Holmlid L. 2015a, 2015b, 2017b). This type of experiment observes the formation and decay of intermediate particles (mesons) in a beam of particles initiated by a laser pulse in real time, not by particle detection in complex detector arrays used by other groups (Burcham and Jobes 1995). This method is novel since such large meson fluxes have not been employed before, and also since it gives a direct particle signal which can be studied by parameter changes in real time. This means that it is possible optimize the meson production more easily than in large-scale experiments. The number of mesons observed in each laser pulse is as large as 10^{15}, which seems to be highest meson intensity used anywhere in the world. A typical formation and decay event is shown in Fig. 7. It should be noted that the direct signal current is in the several mA range without any amplification and without a PMT or similar device. The large current observed could partially be due to a large secondary electron emission coefficient, such that each meson or muon ejects around 10 electrons from the metal collector.

Below, the nuclear reactions are summarized starting with the most long-lived particles observed and moving on to shorter decay times, finally reaching the short-lived neutral kaons and neutral pions. All different mesons and leptons with a lifetime longer than a few ns have been observed (of course excluding neutrinos), also their antiparticles. Of course, the

distinction between the particles and their anti-particles is sometimes quite difficult to make for example for the neutral kaons K_S^0 and K_L^0, which are linear combinations of both (Burcham and Jobes1995; Griffiths 2010). This means that both positive and negative pions $\pi^{\pm}$ (their respective antiparticles) and negative and positive muons $\mu^{\pm}$ (their respective antiparticles) are formed in the kaon decay. It is however not yet known if both positive and negative kaons $K^{\pm}$ are formed in the experiments.

8.1. Active clusters

The known properties of the H(0) material should of course be used to specify better which the basic properties are of the nuclear processes in H(0). The two main types of clusters in H(0) described above are the chain clusters $H_{2N}(0)$ and the small clusters $H_3(0)$ and $H_4(0)$. The small clusters are not superfluid, while the chain clusters are superfluid and also show a Meissner effect at room temperature (Andersson, Holmlid and Fuelling 2012; Holmlid and Fuelling 2015). The superfluid properties of the chain clusters can be observed in experiments where the temperature of the H(0) emitter is varied, and the H(0) on the surface is sampled by laser pulses giving time-of-flight spectra. Such experiments show that the superfluid chain clusters disappear above a transition temperature of few hundred K which depends on the kind of atom (p or D) and on the surface material (Holmlid and Kotzias 2016). However, the small clusters still exist on the surface at high temperature as shown in Fig. 21, and the intermediate mesons ejected are also formed above the transition temperature (Holmlid 2019). Such experiments indicate directly that the nuclear processes giving the mesons take place in the small clusters $H_3(0)$ and $H_4(0)$. This is as expected, since the superfluid chain clusters will be able to transport energy rapidly and thus may not be so easily influenced by laser radiation. Thus the nuclear processes take place primarily in the small clusters $H_3(0)$ and $H_4(0)$. The number of H atoms involved is thus only three or four, and there is no large mass acting to

keep the reacting H atoms in place. The spin state of these small clusters is not known, but it appears likely that the state $s = 1$ must be reached for the small cluster before the nuclear processes take place, for example by tunneling from the close distance of 0.56 pm at $s = 1$. If this process down to $\rightarrow s = 1$ is required to start the nuclear processes, it is also quite unlikely that the chain clusters are involved since that would mean a transfer to $s = 1$ for a majority of the atoms in a large cluster. In fact, no clear evidence exists from CE experiments that chain clusters can transfer down to state $s = 1$ thus to the state with only electron spin and no orbiting motion of the electrons in the clusters. This may be the main reason why the chain clusters are not involved in the nuclear processes in H(0), at least not with laser-induction.

8.2. Heat generation

Several different types of high-energy particles are generated by the laser-pulse interaction in H(0), as described above. Most of these particles are penetrating and do not stop close to the laser target. To test the possibility of local heat generation despite this, an experiment was designed with an enclosure (copper cylinder) around the laser target with H(0) (Holmlid 2015c). The temperature of the enclosure was measured during experiments with variable laser energy and gas pressure. Only D_2 gas was used to optimize the heat generation by giving the possibility of D+D fusion. Thus, the results may be due to nuclear fusion and not only due to (at that time) unknown annihilation-like nuclear processes. Even under these conditions when most high-energy particles could not be contained in the enclosure, an excess heat was observed in the copper cylinder (Holmlid 2015c). The fact that high-energy particles left the enclosure was also described in this report. The results show clearly that excess heat can be generated by the laser impact on D(0), partly due to nuclear fusion, and that further energy generating processes giving even higher energy exist.

The nuclear fusion processes in D(0) had been studied in another publication previous to the heat measurements. That study was done by TOF measurements using a PMT for sensitive particle measurements (Olofson and Holmlid 2014b). All particles involved in D+D fusion processes were detected but T which indeed was expected to react on forming ^{4}He in the end. Of course, neutrons could not be detected by the PMT detector. Collisional processes of several emitted particles with the small $D_4(0)$ clusters were also detected. Thus, background information that fusion indeed took place under the conditions used for the heat measurements existed in Olofson and Holmlid (2014b) prior to the heat generation experiments in Holmlid (2015c).

8.3. Muons

Muons $\mu^{\pm}$ are the final unstable particles generated from the meson showers. These muons are quite difficult to detect since they are often relativistic and have high energy, often close to their ionization minimum at 100 MeV (Groom, Mokhov and Striganov 2001). This means that the type of experiment used for measuring the mesons (timing experiments) is not suitable to directly observe the muons: instead, the collectors used in those experiments transmit the muons after they have generated or just released secondary electrons in the collectors. Thus, a more radiophysical method using scintillators and special novel converters with energy spectral (MCA) measurements has been used to identify the muons (Holmlid and Olafsson 2015a, 2015b ; Olafsson and Holmlid 2016). With metallic converters, electron-positron showers are created, with the energy spectra similar to beta energy distributions (Holmlid and Olafsson 2015a, 2015b ; Olafsson and Holmlid 2016). The cutoff of the energy spectra is close to 511 keV, thus close to the electron mass, which shows that the process involved is electron-positron pair production (to be published). An example is shown in Fig. 22. Such distributions can be observed both with laser-induction and without, thus

spontaneously from H(0), both from p(0) and D(0) (Holmlid and Olafsson 2015a, 2015b ; Olafsson and Holmlid 2016). The number of muons detected in the experiments is very high even at several meter distance from the generator, several orders of magnitude larger than the ambient muons of cosmic origin from the upper atmosphere. This implies that a fusion reactor using muon catalysis is possible (Holmlid 2017e) and the muon generator for this process has indeed been patented (Holmlid 2017d).

Direct decay-time experiments with muons (to be published) give good agreement with accepted data for muon decay. The result of (2.23±0.05) μs agrees with the best value of 2.20 μs (Patrignani *et al.* 2016).

8.4. Other leptons

When the muons decay, electrons and positrons are generated. These lepton signals can be observed in the timing experiments mainly used for muon identification (Holmlid 2016b) by using detection in a small spatial region (pin collector) after particle separation in a magnetic field. Electron-positron pair production was also studied by TOF methods after particle penetration through metal foils (Olofson and Holmlid 2014a). This type of process is also central for the detection of muons (Holmlid and Olafsson 2015a, 2015b ; Olafsson and Holmlid 2016).

8.5. Pions

Charged pions $\pi^{\pm}$ have decay times of 26 ns, and they decay to muons. Thus, they are easily observed by the meson timing experiments of the same type as used for kaons below with both D(0) and p(0) (Holmlid L. 2015a, 2015b, 2017b) and in section 2.3 above. A typical

experimental result is shown in Fig. 23, where the formation time constant is 12 ns, which agrees with their anticipated formation from decaying charged kaons. The signal observed at the collector is in fact due to muons which are formed by decay of pions moving relatively slowly out from the H(0) generator. So the decay observed is due to the decreasing flux of muons ejected by the pions after the laser pulse (which induces the formation of the pions). The muons eject a large number of secondary electrons at the collector, which gives the measured signal current in the mA range at 1 m distance.

8.6. Kaons

Charged kaons $K^{\pm}$ have decay times of 12.4 ns, and they decay primarily to muons but also to charged and neutral pions (Krane 1988; Burcham and Jobes 1995; Nordling and Österman 1998). They are easily observed by the same type of timing experiments used for pions above. Since they form pions (which have longer decay times), a combined decay of kaons and pions is often observed (Holmlid 2015a, 2015b, 2017b). A typical result of pure charged kaon decay is shown in Fig. 7. The signal observed at the collector is in fact due to muons which are formed by decay of charged kaons moving relatively slowly out from the H(0) generator. So the decay observed is due to the decreasing flux of muons ejected by the decaying kaons after the laser pulse. The muons eject secondary electrons at the collector, which gives the signal current.

Neutral kaons exist in two forms which can transform into each other (oscillate), long-lived kaons K_L^0 (with decay time 52 ns) and short-lived kaons K_S^0 (at approximate decay time 0.1 ns). The long-lived 52 ns kaon decay is easily observed in the timing experiments, as shown in Fig. 24. The signal at the collector is formed in the same way as for the charged kaons, thus by muons ejecting secondary electrons from the collector. The signal from the long-lived

neutral kaon K_L^0 does not normally dominate the decay distributions, probably since there is a relatively small chance of interaction of the resulting muons with the foil collectors due to the geometry. Thus this signal is often just a tail on other decay distributions due to pions and charged kaons. The neutral long-lived kaons K_L^0 can be detected both from H(0) and D(0) (Holmlid 2015a, 2015b, 2017b). The short-lived kaons K_S^0 can be detected relatively easily due to their decay to neutral pions which decay rapidly to high-energy gamma photons. These photons can be detected by particle energy measurements in MCA experiments using plastic or NaI(Tl) scintillators. An example is shown in Fig. 25 with only a metal converter, thus no scintillator. The energy calibration there was done at a few MeV, and thus the energy scale is not very accurate, however, the very high energy of the order of 50 MeV is apparent. Just a fraction of the gamma photon energy from the decay of the neutral pions stays in the PMT, so the energy observed is far from the total energy released.

8.7. Meson showers

The kaons and pions detected are all ejected from the H(0) generator by the laser pulse in the timing experiments. It is not possible yet to observe if also D mesons are involved, or further such details of the process. Since both p(0) and D(0) give similar results, it is concluded that the two interacting nuclei are protons in the ultra-dense hydrogen phase, with the electrons very close to the nuclei. When the spin state $s = 1$ is influenced by the laser pulse, a spin flip of one of the spins is possible so that the total spin of the two coupled electrons becomes zero so they can exist at very short relative distance. This may mean a transient configuration of the electrons between the protons, which will increase the probability of tunneling of the two protons. Alternatively, the electrons may get so close to the protons that transient "quasi-neutrons" are formed which can take part in the quark transformation processes, forming

kaons and pions from the two nucleons. The exoergic energetics of the process to three kaons is quite clear as

$$p + p \rightarrow 3\ K \qquad 2\times938\ MeV - 3\times497\ MeV = 385\ MeV$$

This means that besides the kaons also various leptons like muons may be formed, without violating the quark number conservation. The kaons contain strange quarks which must be generated from the existing quarks: the energy for this is available but the detailed processes are not yet known. Other particles which could be intermediates are D mesons and tau leptons, since both particle types have energy close to two protons.

9. Condensation to H(0)

The energy of condensation released during formation of H(0) is considerable. In the state s = 2, the bonding energy per H-H pair is of the order of 1 keV (Holmlid 2013a). This means that the condensation energy is of the order of 100 MJ mol^{-1} H_2, or 27 kWh mol^{-1} H_2. Thus an ordinary gas tube containing hydrogen may be able to release MWh in condensation energy. Of course, this process is not very likely to take place spontaneously . After condensation, spontaneous nuclear processes may take place. Both condensation and spontaneous nuclear processes may be the source of the excess heat observed in the so called "cold fusion" or LENR experiments (Storms 2007, 2014). That condensation energy may be the source of the energy in "cold fusion" was pointed out by Winterberg (2010a,b) and by Mayer and Reitz (2012, 2014).

As discussed above, the formation of H(0) goes over states H(l) and down to H(1). The transfer from H(1) to H(0) is quite complex, since the energy given off by the H(0) cluster formation will mainly be taken up as rotational energy in the clusters. Due to their super properties, they will not easily transfer or lose this energy to the surroundings. This process is

included in Fig. 12, and this figure indicates that the higher state H(1) will be reformed, if the excess condensation energy cannot be removed. Thus, the spontaneous condensation to H(0) is normally a slow process.

10. Where to find H(0)

H(0) is likely to exist where hydrogen is abundant and either catalysts or a long time of undisturbed existence have had a chance to transfer hydrogen to H(0). This means that interstellar space and stars are places to expect H(0). Of course, it could be considered to be quite difficult to observe H(0) by optical spectroscopic methods due to its strong bonding, even if both gamma and radio frequency observations may become possible. In fact, spectroscopy has already given results: good agreement of the rotational spectroscopy results (Holmlid 2017a, 2018a) with the ERE (extended red emission) spectra in space was found and recently published (Holmlid 2018b). This means that H(0) exists in many objects in space, and also in the interstellar medium (ISM). Gamma spectroscopy may also be a useful method.

It is even possible to use CE (Coulomb explosion) based methods in space to identify H(0). This has been possible for the flux of H atoms from the Sun, which is the so called proton solar wind. There exist at least two different components of the proton solar wind from the Sun, the so-called fast and slow winds. Experimental studies of the H fragments from $s = 1$ in H(0) give good agreement with these solar winds (Holmlid 2017c). It is also likely that the very high temperature in the corona is due to nuclear processes in H(0). This high temperature is otherwise not explainable, which has been noted previously (wikipedia 2018) .

11.Conclusions

The very short interatomic distances in ultra-dense hydrogen H(0) have been verified by at least three independent methods, CE laser-based TOF and TOF-MS, rotational emission spectroscopy in the visible range, and laser-induced annihilation-like nuclear processes which eject meson showers. The D-D distance in the D(0) clusters at s = 3 is equal to 5.052 ± 0.003 pm from rotational spectroscopy thus with a precision of a few femtometers, which can be recalculated to s = 2, giving 2.245± 0.003 pm. The theoretical description of H(0) is based on it being the lowest energy (most dense) form of matter with the distance scale given by r_q, the quantum electron radius $r_q = \hbar/2m_e c$ = 0.1931 pm. H(0) has the possibility to become excited into the highest energy form of matter which is superfluid and superconductive with the distance scale given by the London penetration depth $\lambda_L = 137a_0$. Of course, there is also a close relation to the intermediate energy form of matter which includes ordinary matter but which in this case is even better exemplified by ordinary Rydberg Matter, with the distance scale given by the Bohr radius a_0. The existence of a mixed spin quantum number s which determines the structure of H(0) has been demonstrated, with the main contribution from the electron spin and with strong coupling to the vibrational motion in the H(0) clusters. A general formula for the relation between the angular momenta in H(0) and ordinary Rydberg Matter and the interatomic distances has been found, The so called dimensional factor has a value close to 2.90 for both ultradense hydrogen and ordinary Rydberg Matter. The chain clusters $H_{2N}(0)$ have super properties (for example a Meissner effect due to superconductivity), while the small clusters $H_3(0)$ and $H_4(0)$ do not have super properties but are the ones in which the nuclear processes take place at s =1.

Acknowledgment

Parts of the equipment used for the experimental studies have been built with the support of GU Ventures AB, the holding company at the University of Gothenburg. I thank my wife Ulla Holmlid for help with finishing this paper after my recent stroke.

References

M. Andersson, J. Wang and L. Holmlid 1996, "Angular resolved desorption of potassium ions from basal graphite surfaces: ionization of Rydberg species with and without a K beam". J. Chem. Soc., Faraday Trans. 92 (1996) 4581-4588.

Andersson L., Olsson J.O. and Holmlid L. 1986, "Surface ionization at atmospheric pressure: partial melting of alkali salt particles". Langmuir 2, 594-599.

Andersson P.U. and Holmlid L. 2010, "Deuteron energy of 15 MK in a surface phase of ultra-dense deuterium without plasma formation: temperature of the interior of the Sun". Phys. Lett. A 374, 2856–2860 DOI: 10.1016/j.physleta.2010.03.009

Andersson P.U. and Holmlid L. 2011, "Superfluid ultra-dense deuterium D(-1) at room temperature". Phys. Lett. A 375, 1344–1347. doi:10.1016/j.physleta.2011.01.035.

Andersson P.U. and Holmlid L. 2012a, "Cluster ions D_N^+ ejected from dense and ultra-dense deuterium by Coulomb explosions: fragment rotation and D^+ backscattering from ultra-dense clusters in the surface phase**".** Int. J. Mass Spectrom. 310, 32-43.

Andersson P.U. and Holmlid L. 2012b, "Fast atoms and negative chain cluster fragments from laser-induced Coulomb explosions in a super-fluid film of ultra-dense deuterium D(-1)". Phys. Scr. 86, 045601. doi:10.1088/0031-8949/86/04/045601

Andersson P.U., Holmlid L., and Fuelling S.R. 2012, "Search for superconductivity in ultra-dense deuterium D(-1) at room temperature: depletion of D(-1) at field strength > 0.05 T". J. Supercond. Novel Magn. 25, 873-882.DOI: 10.1007/s10948-011-1371-6.

Andersson P.U., Lönn B. and Holmlid L. 2011, "Efficient source for the production of ultra-dense deuterium D(-1) for laser-induced fusion (ICF)".
Rev. Sci. Instrum. 82, 013503. doi:10.1063/1.3514985.

S. Badiei and L. Holmlid (2002a), "Rydberg Matter of K and N_2: angular dependence of the time-of-flight for neutral and ionized clusters formed in Coulomb explosions".

Int. J. Mass Spectrom. 220 (2002) 127-136.

S. Badiei and L. Holmlid (2002b), “Neutral Rydberg Matter clusters from K: extreme cooling of translational degrees of freedom observed by neutral time-of-flight”. Chem. Phys. 282 (2002) 137-146.

Badiei S., Andersson P. U. and Holmlid L. 2009, “High-energy Coulomb explosions in ultra-dense deuterium: Time-of-flight mass spectrometry with variable energy and flight length”. Int. J. Mass Spectrom. 282, 70-76 doi:10.1016/j.ijms.2009.02.014.

Badiei S., Andersson P.U. and Holmlid L. 2010a, “Laser-induced variable pulse-power TOF-MS and neutral time-of-flight studies of ultra-dense deuterium”. Phys. Scripta 81, 045601. doi: 10.1088/0031-8949/81/04/045601

Badiei S., Andersson P.U. and Holmlid L. 2010b, “Production of ultra-dense deuterium, a compact future fusion fuel”. Appl. Phys. Lett. 96, 124103. doi:10.1063/1.3371718

Badiei S.and L. Holmlid 2004, “Experimental observation of an atomic hydrogen material with H - H bond distance of 150 pm suggesting metallic hydrogen”. J. Phys.: Condens. Matter 16 (2004) 7017-7023.

Badiei S. and Holmlid L. 2006, “Experimental studies of fast fragments of H Rydberg matter”. J. Phys. B: At. Mol. Opt. Phys. 39, 4191-4212.

Burcham, W. E. & Jobes, M. 1995, "*Nuclear and Particle Physics*, " (Pearson, Harlow).

Norman D. Cook 2010, "Models of the Atomic Nucleus: Unification Through a Lattice of Nucleons", 2nd ed., Springer , Berlin, 2010.

Engvall K., Kotarba A. and Holmlid L. 1999, "Long-range diffusion of K promoter on an ammonia synthesis catalyst surface - ionization of excited potassium species in the sample edge fields". J. Catal. 181, 256-264.

K. Engvall and L. Holmlid, "Field ionization of excited alkali atoms emitted from catalyst surfaces". Appl. Surface Sci. 55 (1992) 303-308

K. Engvall, A. Kotarba and L. Holmlid 1994, "Emission of excited potassium species from an industrial iron catalyst for ammonia synthesis". Catal. Letters 26 (1994) 101-107.

K. Engvall, A. Kotarba and L. Holmlid 1999, "Long-range diffusion of K promoter on an ammonia synthesis catalyst surface - ionization of excited potassium species in the sample edge fields". J. Catal. 181 (1999) 256-264.

Fröchtenicht R., Toennies J.P., Vilesov A. 1994, " High-resolution infrared spectroscopy of SF_6 embedded in He clusters" Chemical Physics Letters 229, l-7.

Gallagher T. F. 1994, "*Rydberg Atoms*" (Cambridge University Press, Cambridge,).

Goyal S., Schutt D. L., and Scoles G., 1994, "Vibrational spectroscopy of sulfur hexafluoride attached to helium clusters", Phys. Rev. Lett. 73, 2512.

Griffiths D. 2010, "*Introduction to elementary particles*," 2nd ed., Wiley-VCH, Weinheim

E. Groom, N. V. Mokhov and S. Striganov 2001, "Muon stopping power and range tables 10 MeV-100 TeV", Atomic Data and Nuclear Data Tables,78(2), Pages 183-356 L BNL-44742).

T. Guénault, 2003, "*Basic superfluids*", (Taylor and Francis, London).

Haken H. and Wolf H.C. 2005, " *The physics of atoms and quanta*, " 7th ed., Springer, Berlin.

D. Hestenes (1990). "The zitterbewegung interpretation of quantum mechanics". *Foundations of Physics*. **20** (10): 1213–1232.

Hirsch, J.E. 2010, "Hole core in superconductors and the origin of the Spin Meissner effect" Physica C **470**, 635.

Hirsch J.E. 2012, "The origin of the Meissner effect in new and old superconductors," Physica Scripta 85, 035704.

Hollas J.M., 2004, "*Modern spectroscopy*", 4th ed., Wiley, Hoboken.

Holmlid L., K. Engvall, C. Åman and P. G. Menon 1993, "A new approach to loss of alkali promoter from industrial catalysts: importance of excited states of alkali". "New Frontiers in

Catalysis", Proceedings of the 10th International Congress on Catalysis (eds. L. Guczi, F. Solymosi and P. Tétényi), Akadémiai Kiadó, Budapest 1993, p. 795-807.

Holmlid L. 1998a, "Classical energy calculations with electron correlation of condensed excited states - Rydberg Matter". Chem. Phys. 237, 11-19.

Holmlid L. 1998b, "Complex kinetics of desorption and diffusion. Field reversal study of K excited-state desorption from graphite layer surfaces". J. Phys. Chem. A 102, 10636-10646.

L. Holmlid 1998c, "Nanosecond switching, field reversal evidence of Rydberg atom desorption from surfaces". Chem. Phys. 230 (1998) 327-344.

L. Holmlid 2003, "Rydbergsmateria - dagbok från labbet". Forskning och Framsteg 2003, No. 4, p. 14-17.

L. Holmlid (2004), "Optical stimulated emission transitions in Rydberg Matter observed in the range 800 - 14000 nm". J. Phys. B: At. Mol. Opt. Phys. 37 (2004) 357-374.

Holmlid L. 2007, "Precision bond lengths for Rydberg Matter clusters K_{19} in excitation levels $n = 4$, 5 and 6 from rotational radio-frequency emission spectra".
Mol. Phys 105, 933-939.

Holmlid L. 2008a, "Rotational spectra of large Rydberg Matter clusters K_{37}, K_{61} and K_{91} give trends in K-K bond distances relative to electron orbit radius".
J. Mol. Struct. 885, 122-130.

Holmlid L. 2008b, "Clusters H_N^+ ($N = 4$, 6, 12) from condensed atomic hydrogen and deuterium indicating close-packed structures in the desorbed phase at an active catalyst surface". Surf. Sci. 602, 3381–3387.

Holmlid L. 2010a, "Nanometer interatomic distances in Rydberg Matter clusters confirmed by phase-delay spectroscopy". J. Nanopart. Res. 12, 273-284.
DOI 10.1007/s11051-009-9605-2.

Holmlid L. 2010b, "Common forms of alkali metals - new Rydberg Matter clusters of potassium and hydrogen". J. Clust. Sci 21, 637-653. DOI: 10.1007/s10876-010-0291-0.

Holmlid L. 2011a, "Large ion clusters H_N^+ of Rydberg Matter: stacks of planar clusters H_7". Int. J. Mass Spectrom. 300, 50-58. doi:10.1016/j.ijms.2010.12.008.

Holmlid L. 2011b, "High-charge Coulomb explosions of clusters in ultra-dense deuterium D(-1)". Int. J. Mass Spectrom. 304, 51–56. doi: 10.1016/j.ijms.2011.04.001.

Holmlid L. 2011c, "Sub-nanometer distances and cluster shapes in dense hydrogen and in higher levels of hydrogen Rydberg Matter by phase-delay spectroscopy". J. Nanopart.Res. 13, 5535-5546. DOI 10.1007/s11051-011-0543-4.

Holmlid L. 2012a, "Deuterium clusters D_N and mixed K-D and D-H clusters of Rydberg Matter: high temperatures and strong coupling to ultra-dense deuterium".
J. Clust. Sci. 23, 95-114.DOI 10.1007/s10876-011-0387-1.

Holmlid L. 2012b, "Experimental studies and observations of clusters of Rydberg matter and its extreme forms". Invited review. J. Cluster Sci. 23, 5-34.
DOI: 10.1007/s10876-011-0417-z.

Holmlid L. 2013a, "Excitation levels in ultra-dense hydrogen p(-1) and d(-1) clusters: structure of spin-based Rydberg Matter".
Int. J. Mass Spectrom. 352, 1- 8. DOI: 10.1016/j.ijms.2013.08.003.

Holmlid L. 2013b, "Laser-mass spectrometry study of ultra-dense protium p(-1) with variable time-of-flight energy and flight length".Int. J. Mass Spectrom. 351, 61-68. DOI: 10.1016/j.ijms.2013.04.006.

Holmlid L. 2014, "Ultra-dense hydrogen H(-1) as the cause of instabilities in laser compression-based nuclear fusion".
J. Fusion Energy 33,348-350.DOI: 10.1007/s10894-014-9681-x.

Holmlid L. 2015a, “MeV particles in a decay chain process from laser-induced processes in ultra-dense deuterium D(0)”.
Int. J. Modern Phys. E 24, 1550026. DOI: 10.1142/S0218301315500263.

Holmlid L. 2015b,“Nuclear particle decay in a multi-MeV beam ejected by pulsed-laser impact on ultra-dense hydrogen H(0)”.
Int. J. Modern Phys. E 24, 1550080. DOI: 10.1142/S0218301315500809.

Holmlid L. 2015c, “Heat generation above break-even from laser-induced fusion in ultra-dense deuterium”. AIP Advances 5, 087129. doi: 10.1063/1.4928572.

Holmlid L. 2016b, “Leptons from decay of mesons in the laser-induced particle pulse from ultra-dense protium p(0)”. Int. J. Modern Phys. E 25, 1650085. DOI: 10.1142/S0218301316500853.

Holmlid L. 2017a, “Emission spectroscopy of IR laser-induced processes in ultra-dense deuterium D(0): Rotational transitions with spin values s = 2, 3 and 4”.
J. Mol. Struct. 1130, 829–836. Doi: 10.1016/j.molstruc.2016.10.091.

Holmlid L. 2017b, “Mesons from laser-induced processes in ultra-dense hydrogen H(0)”.
PLOS ONE 12, e0169895. doi:10.1371/journal. pone.0169895. and arXiv.

Holmlid L. 2017c, “The solar wind proton ejection mechanism: experiments with ultra-dense hydrogen agree with observed velocity distributions”.
J. Geophys. Res. - Space Phys. 122, 7956–7962. doi: 10.1002/2017JA024498.

Holmlid L. 2017d, “Apparatus for generating muons with intended use in a fusion reactor”.
Swedish patent application 1651504-1 submitted 2016-11-17. Patent nr SE 539684 C 2 granted, published 2017-10-31.

Holmlid L. 2017e, “Neutrons from muon-catalyzed fusion and from capture processes in an ultra-dense hydrogen H(0) generator**”.** Fusion Science and Technology, https://doi.org/10.1080/15361055.2017.1421366.

Holmlid L. 2018a, “Rotational emission spectroscopy in ultra-dense hydrogen p(0) and pxDy(0): groups pN, pD2, p2D and (pD)N”. Journal of Molecular Structure 1173, 567-573 (2018) doi;10.1016/j.molstruc.2018.06.116.

Holmlid L. 2018b, “ Ultra-dense hydrogen H(0) as stable dark matter in the Universe: extended red emission spectra agree with rotational transitions in H(0)**.”** Astrophysical Journal 866:107 (4pp), doi: 10.3847/1538-4357/aadda1

L. Holmlid 2019, “Laser-induced nuclear processes in ultra-dense hydrogen take place in small non-superfluid $H_N(0)$ clusters”. DOI: 10.1007/s10876-018-1480-5. Journal of Cluster Science, 30(1), 235-242.

L. Holmlid, K. Engvall, C. Åman and P. G. Menon (1993), "A new approach to loss of alkali promoter from industrial catalysts: importance of excited states of alkali". "New Frontiers in Catalysis", Proceedings of the 10th International Congress on Catalysis (eds. L. Guczi, F. Solymosi and P. Tétényi), Akadémiai Kiadó, Budapest 1993, p. 795-807.

Holmlid L. and Fuelling S.R. 2015, “Meissner effect in ultra-dense protium p(l=0, s=2) at room temperature: superconductivity in large clusters of spin-based matter”.
J. Cluster Science 26, 1153-1170. DOI 10.1007/s10876-014-0804-3

Holmlid L. and Kotzias B. 2016, “Phase transition temperatures of 405-725 K in superfluid ultra-dense hydrogen clusters on metal surfaces”. AIP Advances 6, 045111. doi: 10.1063/1.4947276.

L. Holmlid and P.G. Menon 2001, “Emission and Loss of Potassium Promoter from Styrene Catalysts: Studies by UHV/Molecular-Beam and Laser Techniques”.
Appl. Catal. A. 212 (2001) 247-255.

Holmlid L. and Olafsson S. 2015a, “Spontaneous ejection of high-energy particles from ultra-dense deuterium D(0)”. Int. J. Hydr. Energy 40, 10559-10567. DOI: 10.1016/j.ijhydene.2015.06.116.

Holmlid L. and Olafsson S. 2015b, “Muon detection studied by pulse-height energy analysis: novel converter arrangements”.Rev. Sci. Instrum. 86, 083306, DOI: 10.1063/1.4928109.

Holmlid L. and Olafsson S. 2016, “Charged particle energy spectra from laser-induced processes: nuclear fusion in ultra-dense deuterium D(0)”.

Int. J. Hydrogen Energy 41, 1080-1088. doi:10.1016/j.ijhydene.2015.10.072.

Hora H. 2000, "*Plasmas at High Temperature and Density",* Springer, Heidelberg 1991; 2nd ed. S. Roderer, Regensburg.

Kaminsky M. 1965, "*Atomic and Ionic Impact Phenomena on Metal Surfaces*, " Springer, Berlin.

Klempt, E., Batty, C., & Richard, J.-M. 2005, "The antinucleon-nucleon interaction at low energy: annihilation dynamics, " *Phys. Rep.* **413**, 197.

A. Kotarba, K. Engvall, J.B.C. Pettersson, M. Svanberg and L. Holmlid, 1995 "Angular resolved neutral desorption of potassium promoter from surfaces of iron catalysts". *Surface Sci.* 342 (1995) 327-340.

A. Kotarba, A. Baranski, S. Hodorowicz, J. Sokolowski, A. Szytula, and L. Holmlid, “Stability and excitation of potassium promoter in iron catalysts - the role of $KFeO_2$ and $KAlO_2$ phases”. *Catal. Letters* 67 (2000) 129-134.

A. Kotarba and Holmlid L. 2009, “Energy-pooling transitions to doubly excited K atoms at a promoted iron-oxide catalyst surface: more than 30 eV available for reaction”. *Phys. Chem. Chem. Phys*. 11, 4351-4359. DOI: 10.1039/b817380j..

Krane K. S., 1988, "*Introductory Nuclear Physics*," (Wiley, Hoboken).

L’Annunziata M. F. 2012, "Handbook of Radioactivity Analysis", Elsevier, Chapter 1: "Radiation Physics and Radionuclide Decay, "

Manykin É. A., Ozhovan M. I., and Poluéktov P. P. 1980. "Transition of an excited gas to a metallic state, " Sov. Phys. Tech. Lett. 6, 95.

Manykin É. A., Ozhovan M. I., and Poluéktov P. P. 1981. "On the collective electronic state in a system of strongly excited atoms." Sov. Phys. Dokl. 26, 974.

Manykin É. A., Ozhovan M. I., and Poluektov P. P. 1983. "Theory of the condensed state in a system of excited atoms. Sov. Phys. JETP 57, 256.

Mayer F. J. and Reitz J. R. 2012, "Electromagnetic Composites at the Compton Scale, " Int. J. Theor. Phys. 51 (2012) 322–330. DOI 10.1007/s10773-011-0959-8.62

Mayer F. J. and Reitz J. R.2014, "Thermal energy generation in the earth," Nonlin. Processes Geophys., 21, 367–378, 2014

M. Muhler, R. Schlögl, and G. Ertl (1992). The nature of the iron oxide-based catalyst for dehydrogenation of ethylbenzene to styrene 2. Surface chemistry of the active phase. J. Catal. 138, 413.

Nordling, C. & Österman, J. 1988, "*Physics Handbook,* " (Studentlitteratur, Lund, Sweden).

Nyman G., Holmlid L. and Pettersson J.B.C. 1990, "Surface scattering of NO from graphite: A statistical description of energy distributions". J. Chem. Phys. 93, 845-853.

Olafsson S. and Holmlid L. 2016, "Rydberg phases of hydrogen and low energy nuclear reactions". Bull. Am. Phys. Soc. 2016/4/16. BAPS.2016.APR.E9.9.

Olofson F. and Holmlid L. 2012, "Superfluid ultra-dense deuterium D(-1) on polymer surfaces: structure and density changes at a polymer-metal boundary".

J. Appl. Phys. 111, 123502; http://dx.doi.org/10.1063/1.4729078

Olofson F. and Holmlid L. 2014a, "Electron-positron pair production observed from laser-induced processes in ultra-dense deuterium D(-1)".

Laser Part. Beams 32, 537-548. doi:10.1017/S0263034614000494.

Olofson F. and Holmlid L. 2014b, "Time-of-flight of He ions from laser-induced processes in ultra-dense deuterium D(0)".

Int. J. Mass Spectrom. 374, 33–38. DOI: 10.1016/j.ijms.2014.10.004.

B. E. R. Olsson, R. Svensson, and J. Davidsson (1995). "A spectroscopic investigation of the inter-electrode region in an open caesium plasma diode", J. Phys. D Appl. Phys. 28, 479.

C. Patrignani *et al.* (Particle Data Group), 2016, " Review of particle physics," Chin. Phys. C 40 () 100001. (URL: http://pdg.lbl.gov).

Pettersson J.B.C., Holmlid L. and Möller K. 1989, "Alkali promotor function in heterogeneous catalysis: possibility of interaction in the form of Rydberg states". Appl. Surface Sci. 40, 151-154.

Pettersson J.B.C., Nyman G. and Holmlid L. 1988, "A classical trajectory study of inelastic scattering of NO from graphite surfaces: Rotational energy distributions". J. Chem. Phys. 89, 6963-6971

J.B.C. Pettersson and L. Holmlid 1989, "Rydberg states of cesium in the flux from surfaces at high temperatures". Surface Sci. 211 (1989) 263-270.

Reif F. 1965, "*Fundamentals of Statistical and Thermal Physics*" (McGraw-Hill, New York,).

Schrödinger E. 1930 *Sitz.ber., Preuss. Akad. Wiss. Phys.-Math.* **24** 418

Silfvast W. T. 2008., "*Laser Fundamentals*", Cambridge University Press,

Sorochenko R. L. 1990, in "*Radio recombination lines: 25 years of investigation*, " M. A. Gordon, R. L. Sorochenko (eds.), Kluwer, 1990.

P. Stelmachowski, P. Legutko, T. Jakubek, P. Indyka, Z. Sojka, L. Holmlid, A. Kotarba 2015, "Emission of highly excited electronic states of potassium from cryptomelane nanorods". Phys. Chem. Chem. Phys. 17 (2015) 26289-94. DOI: 10.1039/c5cp04108b.

Storms E., 2007,"*The Science of Low Energy Nuclear Reaction*, " World Scientific PublishingCompany, Singapore.

Storms E., 2014,"*The Explanation of Low Energy Nuclear Reaction*", Infinite Energy Press, Concord, NH, USA.

Svensson R. and L. Holmlid (1992), "Temperature studies and plasma probing of a Rydberg matter collector in a thermionic energy converter". Proceedings 27th Intersociety Energy Conversion Engineering Conference, (IECEC 1992, San Diego), Society of Automotive Engineers, Warrendale 1992, Vol. 3, p. 537-542.

Svensson R., Holmlid L. and Lundgren L. 1991, "Semi-conducting low pressure, low temperature plasma of cesium with unidirectional conduction".
J. Appl. Phys. 70, 1489-1492.

Taylor J.B. and Langmuir I. 1933, "The Evaporation of Atoms, Ions and Electrons from Caesium Films on Tungsten", Phys. Rev. 44, (1933) 423.

M. Trebala, W. Bieniasz, L. Holmlid, M. Molenda, and A. Kotarba, 2011"Potassium stabilization in ß-$K_2Fe_{22}O_{34}$ by Cr and Ce doping studied by field reversal method".
Solid State Ionics 192 (2011) 664–667. doi:10.1016/j.ssi.2010.08.004

Wang J. and Holmlid L. 1998, "Planar clusters of Rydberg Matter K_N (N = 7, 14, 19, 37, 61) detected by multiphoton fragmentation time-of-flight mass spectrometry".
Chem. Phys. Letters 295, 500-508.

J. Wang and L. Holmlid (2000), "Formation of long-lived Rydberg states of H_2 at K impregnated surfaces". Chem. Phys. 261 (2000) 481-488.

J. Wang and L. Holmlid (2002), "Rydberg Matter clusters of hydrogen $(H_2)_N^*$ with well defined kinetic energy release observed by neutral time-of-flight".
Chem. Phys. 277 (2002) 201-210.

Wang J., Engvall K. and Holmlid L. 1999, "Cluster K_N formation by Rydberg collision complex stabilization during scattering of a K beam off zirconia surfaces".
J. Chem. Phys. 110, 1212-1220.

wikipedia 2018, Available at:
https://en.wikipedia.org/wiki/Corona#Coronal_heating_problem (Accessed: 22 05 2018)

Winterberg F. 2010a. "Ultradense Deuterium, " J. Fusion Energy 29, 317.

Winterberg F. 2010b. "Ultra-dense deuterium and cold fusion claims", Phys. Lett. A 374, 2766.

V.I.Yarygin (2012), Experimental Studies of Properties of Excited States of Cesium (Rydberg Matter) in the Interelectrode Plasma of a Low-Temperature Thermal to Electric Energy Thermionic Converter, J. Clust. Science 23 (2012) 77-93.

A. H. Zewail (2000), Femtochemistry: Atomic-Scale Dynamics of the Chemical Bond, J. Phys. Chem. A, 2000, 104 (24), 5660–5694, DOI: 10.1021/jp001460h

Åman C., Pettersson J.B.C. and Holmlid L. (1990), "Field ionizable cesium metal clusters from a foil diffusion source". Chem. Phys. 147, 189-197.

C. Åman, J.B.C. Pettersson, H. Lindroth and L. Holmlid (1992), "Visible luminescence from particles on surfaces: Evidence of de-excitation of Rydberg matter".

J. Mat. Research 7 (1992) 100-104.

Table 1. Nominal rotational emission lines from different groups in H(0). a is (Holmlid 2017a), b is (Holmlid 2018a).

nm	p_2	p_3, p_4, D_2	p_6, p_8, D_3, D_4	pD	$(pD)_2$	pD_2	p_2D	Ref.
299.7	s=4 J=3	s=4 J=7	s=2 J=0					a
303.4			s=3 J=4			s=3 J=3		a
316.1							s=3 J=2	
319.7				s=4 J=4	s=4 J=9			a
333.0							s=4 J=8	
337.1					s=3 J=2			
342.6		s=4 J=6						a
355.2					s=4 J=8			b
374.6							s=4 J=7	
379.3	s=3 J=0	s=3 J=1	s=3 J=3					a
399.6	s=4 J=2	s=4 J=5		s=4 J=3	s=4 J=7			a
404.5						s=3 J=2		
428.1						s=4 J=8	s=4 J=6	
456.7					s=4 J=6			b
474.1							s=3 J=1	
479.6		s=4 J=4				s=4 J=7		a
499.5							s=4 J=5	b
505.7			s=3 J=2	s=3 J=0	s=3 J=1			a,b
532.8			s=4 J=8	s=4 J=2	s=4 J=5			a
547.9						s=4 J=6		b
599.5	s=4 J=1	s=4 J=3	s=4 J=7				s=4 J=4	a,b
606.8						s=3 J=1		b
639.3					s=4 J=4	s=4 J=5		
685.1			s=4 J=6					b
749.3							s=4 J=3	b
758.6		s=3 J=0	s=3 J=1					a,b
767.0						s=4 J=4		b
799.2		s=4 J=2	s=4 J=5	s=4 J=1	s=4 J=3			a

Figure captions

Fig. 1. Coulomb interactions in an H_2 pair in ultradense hydrogen H(0) with two hydrogen nuclei and two electrons. Observe that there are four pair-wise attractions and only two pair-wise repulsions, which makes this ensemble a stable, strongly bound entity independent of the distance scale. See further the text for the applicable quantization of the angular momenta involved.

Fig. 2. Common laser-induced TOF peaks from unsupported D(0), thus with kinetic energy only from the CE process. The highest energy at the peaks marked D_3 and D_4 is 630 eV on a D atom. Other peaks are marked with the fragmentation observed. A vertical source for D(0) (Andersson, Lönn and Holmlid 2011) was used with and without D_2 gas. Short 101 mm TOF path.

Fig. 3. Overview of apparatus for CE TOF and TOF-MS experiments with two flight distances, horizontal cut. The thick scintillator used in the outer detector only detects ions while the catcher foil and thin scintillator in the inner detector also detects fast neutrals. The pressure given is base pressure, normal hydrogen pressure is 8×10^{-6} - 1.2×10^{-5} mbar from uncorrected hot-cathode vacuum gauge reading.

Fig. 4. Setup of source and inner detector for some CE TOF and TOF-MS experiments, vertical cut shown. The laser beam is in reality in the horizontal plane where the ion and neutral beam also exist. Due to the catcher foil, also fast neutrals give a signal in this inner detector. Flight distance for neutrals from laser target to catcher foil is 101 mm.

Fig. 5. TOF-MS spectra with variable target voltage (every 50 V) from p(0) on a steel surface, in plots compensated for the target voltage. Long 1120 mm TOF path. Unchanged TOF between spectra means ions with no kinetic energy from CE, shorter TOF at low voltage means large kinetic energy release (KER). The large fragments have around 315 eV kinetic energy from the CE. The p_{30} fragment is transiently negatively charged during the acceleration phase (Holmlid 2013b).

Fig. 6. Rotational emission spectrum from D(0), assigned to $s = 4$, $J = 4$ in agreement with Table 1. One or both of the peaks may be due to pD_2 while p_3 and p_4 are unlikely in the D_2 gas used. The difference in the dimensional factor is only 0.2 %.

Fig. 7. Time-of-flight current muon signal to two collectors in the same direction, with distances from the laser target given. D(0) on a Ta surface. The dashed curves are fitted signals for intermediate mesons with formation time constant τ_1 and decay time constant τ_2, with parameters given. Charged kaon decay is observed at the outer collector and charged pion decay at the inner collector.

Fig. 8. Data from Fig. 7 replotted on energy per mass unit u and velocity scales. The velocity at the outer collector is much higher than at the inner collector, which shows decay of particles in the beam. The muons giving the signal at the outer collector were probably not yet formed when their $K^{\pm}$ precursor mesons passed the inner collector around the peak of that distribution.

Fig. 9. Potential energy for an electron around the center atom in a 19-atom planar close-packed Rydberg matter cluster. Note the circular minimum path around the central atom, with radius 14 au. The distance between the atoms is 40 au, thus a dimensional ratio of approximately 2.9. More results exist in (Holmlid 1998a).

Fig. 10. A short chain cluster $H_{2N}(0)$. Rotation of one H-H pair and the combination to two pairs are indicated. The plane and mode of motion of the electrons with $l = 0$ is unspecified in this figure.

Fig. 11. Scattering of K beam and cluster addition forming Rydberg matter clusters K^*_{N+1} on a zirconia surface. The clusters K^*_N desorb thermally from the surface.

Fig. 12. Relation between H(0) spin states, ordinary H_2 molecules and H(l) Rydberg matter. The transformation between H(0) and H(1) is indicated with a blue arrow. The states reached in H(0) (in red) are highly excited by rotation of the H_2 pairs in the H(0) clusters.

Fig. 13. Time development of D(0) forms during an experimental run with D_2 gas at a catalyst sample. Dense D(0) and D(1) primarily releases small fragments from large clusters (in a dense cloud) while the chain-type clusters (filamentary clusters at lower D(0) density) give two equally large fragments, thus shoing central cleavage of the chain clusters.

Fig. 14. TOF-MS with variable acceleration voltage (every 50 V) from D(0) on stainless steel. The neutral D atoms have energy 500 - 1200 eV, or even more if they are cluster fragments like $D_2(0)$. Laser running at 2 Hz, 100 shots in each spectrum.

Fig. 15. TOF from D(0) on stainless steel, showing contributions from small symmetric clusters. The peaks to the left are due to explosions of small clusters $D_4(0)$ and $D_3(0)$ (Holmlid 2011b). Interference from chain clusters at $s = 2$ is here small due to low laser energy.

Fig. 16. Photo of the atmosphere in the apparatus after laser running for an hour at a few mbar D_2 pressure. An aerosol is observed in the vacuum.

Fig. 17. This is part a movie CIMG00373.mov. Use a program like Apple Quick Time player which makes it possible to step one frame at a time. Laser repetition time 100 ms, each frame is within 1 ms. Light emitting particles move after the laser shot with a few m s^{-1} during 10-20 ms and collide with the chamber walls, still radiating white. Camera Casio Exilim EX-ZR200 mode HS1000 with 224x64 pixels.

Fig. 18. Floating of chain clusters $D_{2N}(0)$ in a magnetic field. With laser beam passing above magnet pole face, no small clusters are observed but only a low intensity of chain clusters and of ordinary Rydberg matter levels D(1). By adjusting the laser beam slightly lower thus partially hitting the edge of the magnet, small clusters $D_3(0)$ and small chain clusters are instead observed.

Fig. 19. Floating of chain clusters $H_{2N}(0)$ above a magnet pole face. The laser beam was parallel to the face. The laser beam was adjusted in height above the pole face. Long TOF path, single-shot spectra measured on an oscilloscope. 20 μs corresponds to p_{20} clusters with 315 eV kinetic energy.

Fig. 20. Destruction of both D(0) and D(1) in a magnetic field, lower spectrum. D(0) on sloping Ta foil in both cases, with magnet below half of the foil. Single-shot first shot spectra.

Fig. 21. TOF spectra for D(0) on a Pt surface with variable temperature. Detector at 45º relative to incoming laser beam. The superfluid chain clusters of D(0) disappear above approximately 525 K, while the small clusters exist even above 900 K.

Fig. 22. Energy spectrum of spontaneous muons from D(0) with 10 mbar D_2 in the vacuum chamber with the D(0) generator. MCA spectra shown with a detector separate from the chamber. The detector consisted of only an Al foil converter and a PMT in a light-tight metal housing. Linear plot and Kurie-type plot giving a cut-off at approximately 530 keV (from calibration with ^{137}Cs). 500 seconds, no laser on.

Fig. 23. Laser-induced charged pions with decay time constant 26 ns from charged kaons with decay time constant 12 ns, decaying to muons which are detected at a foil collector at 1 m distance from the H(0) source. H(0) formed at 0.2 mbar H_2 gas pressure. At time around 100 ns, a contribution from neutral kaons is observed.

Fig. 24. Laser-induced neutral kaon decay with time constant 52 ns, to muons which are detected at 1 m distance at a foil collector. D(0) formed in 0.2 mbar D_2.The first part of the curve is due to charged kaons with decay time constant 12 ns giving pions.

Fig. 25. Energy spectrum from D(0) in apparatus, spontaneous thus with no laser on. The PMT detector is separate from the vacuum chamber, with only a metal converter in front. The

assignment is tentative. Each neutral pion gives two gamma quanta with a sum of at least 135 MeV. Photon energies of the order of 50 MeV are clearly observed.

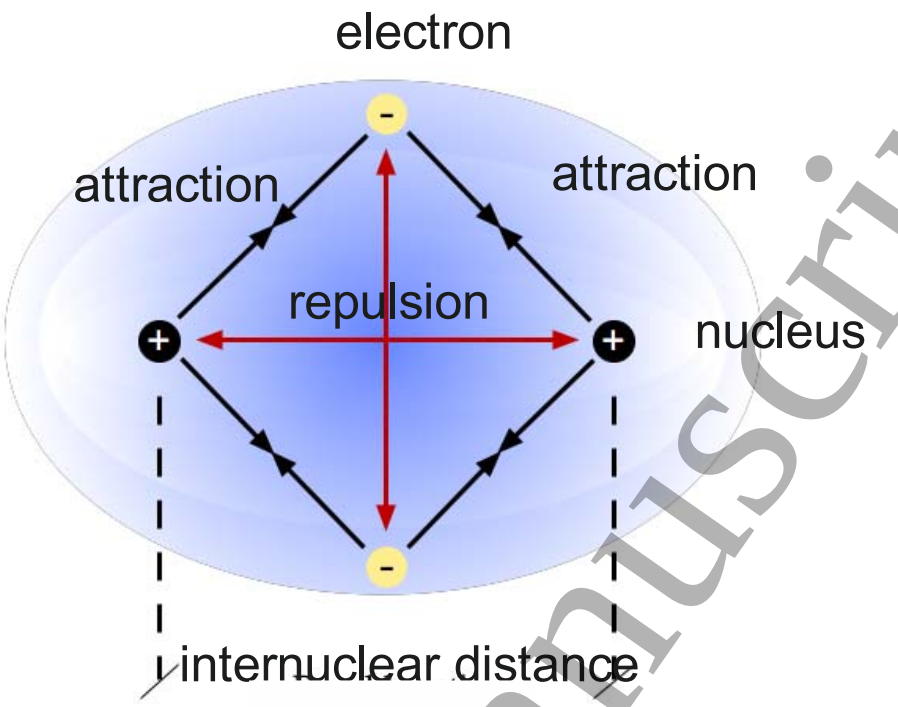

Fig. 1

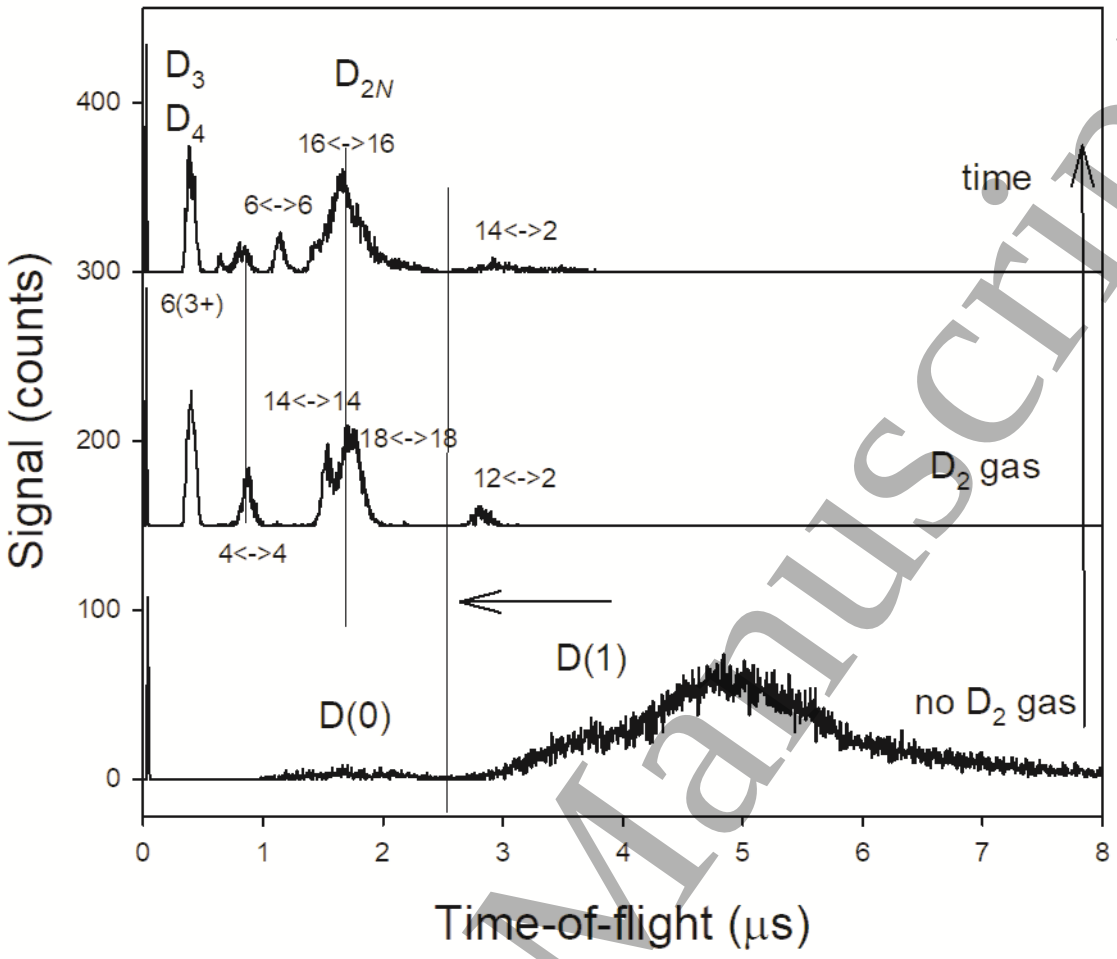

Fig, 2

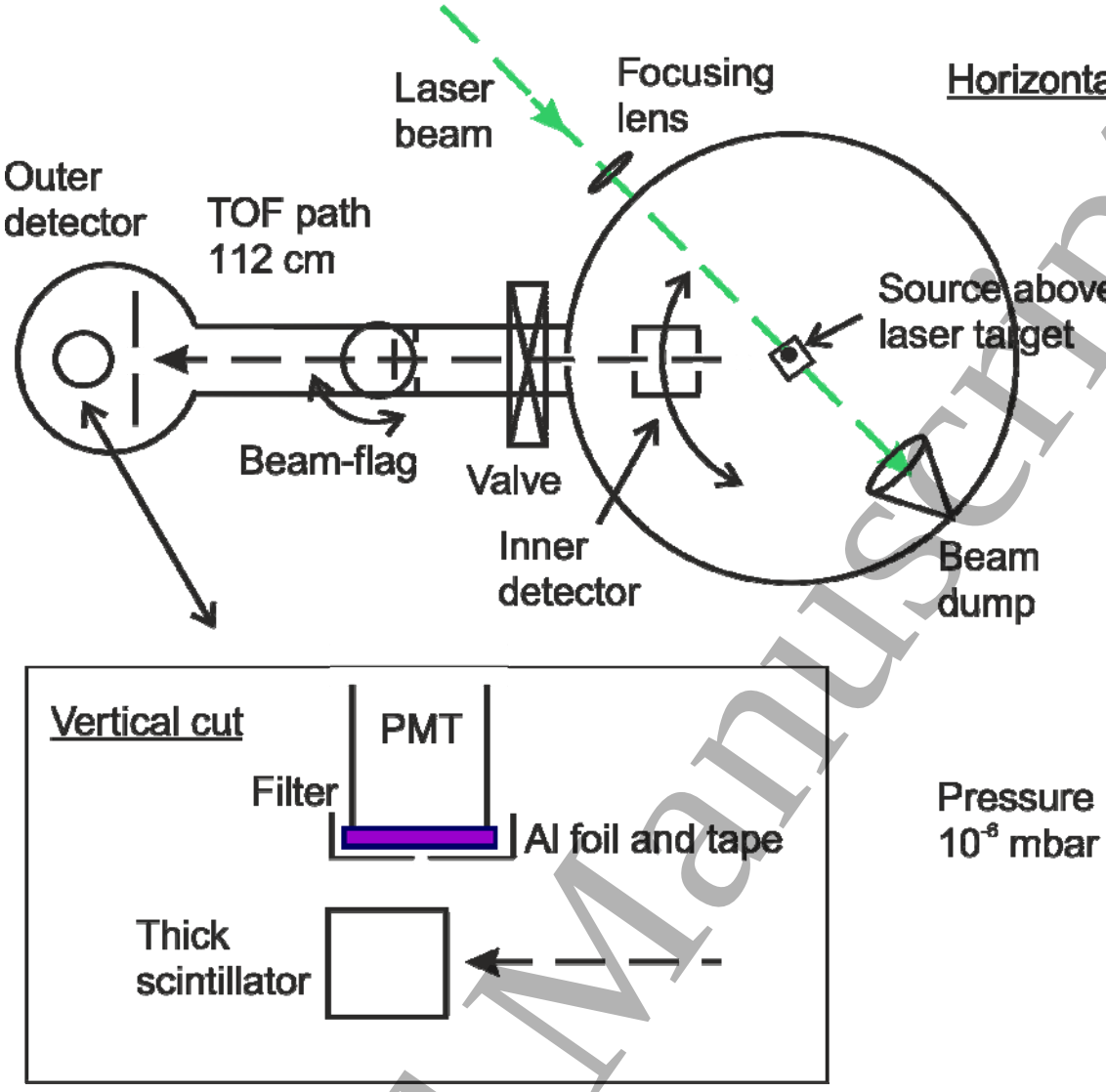

Fig. 3

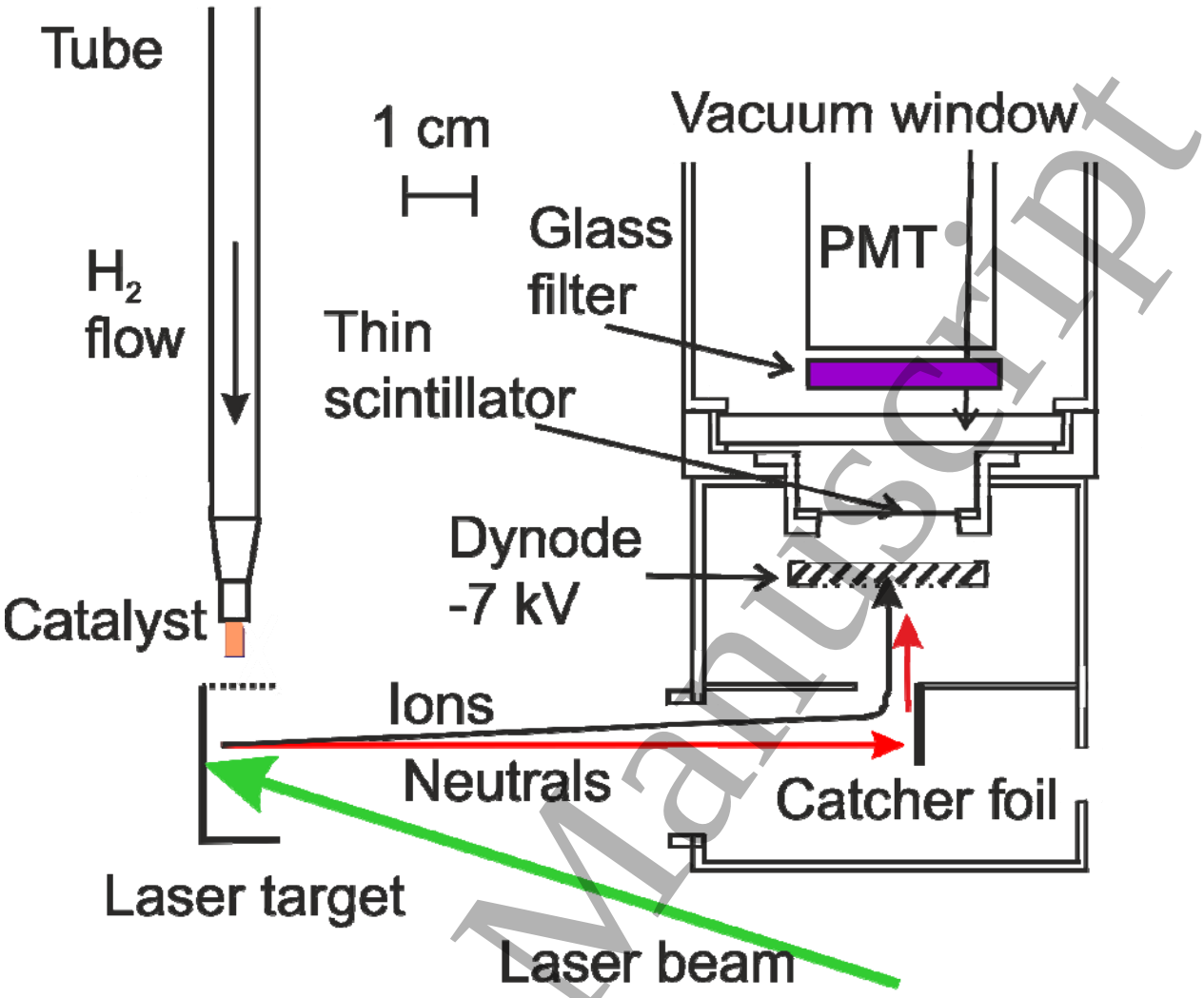

Fig. 4

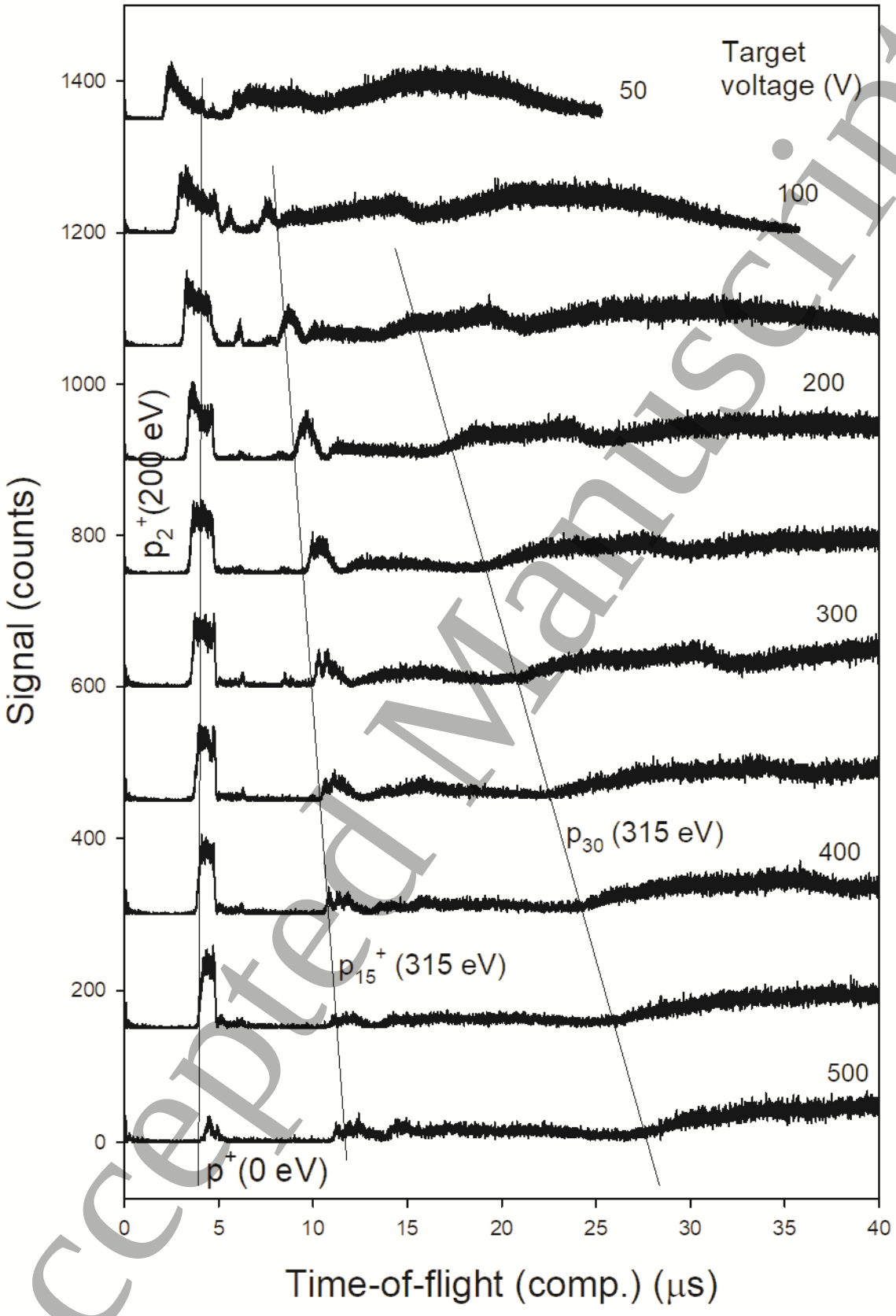

Fig. 5

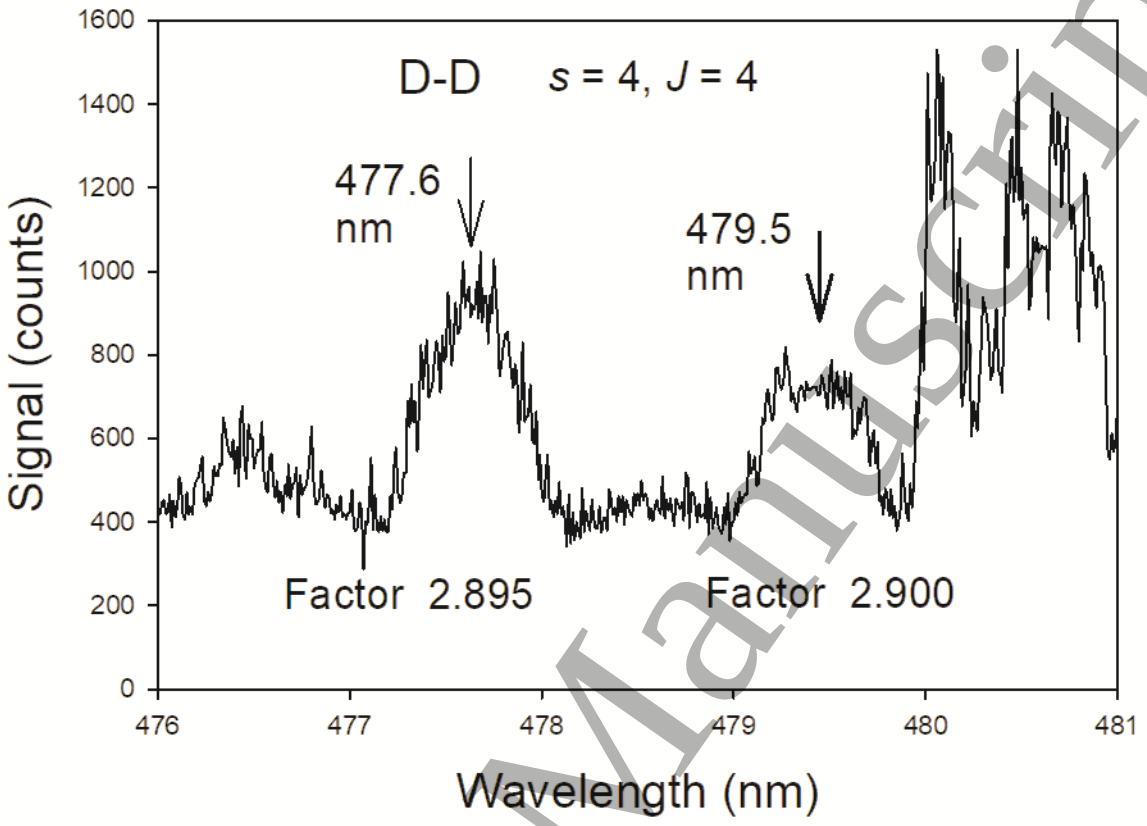

Fig. 6

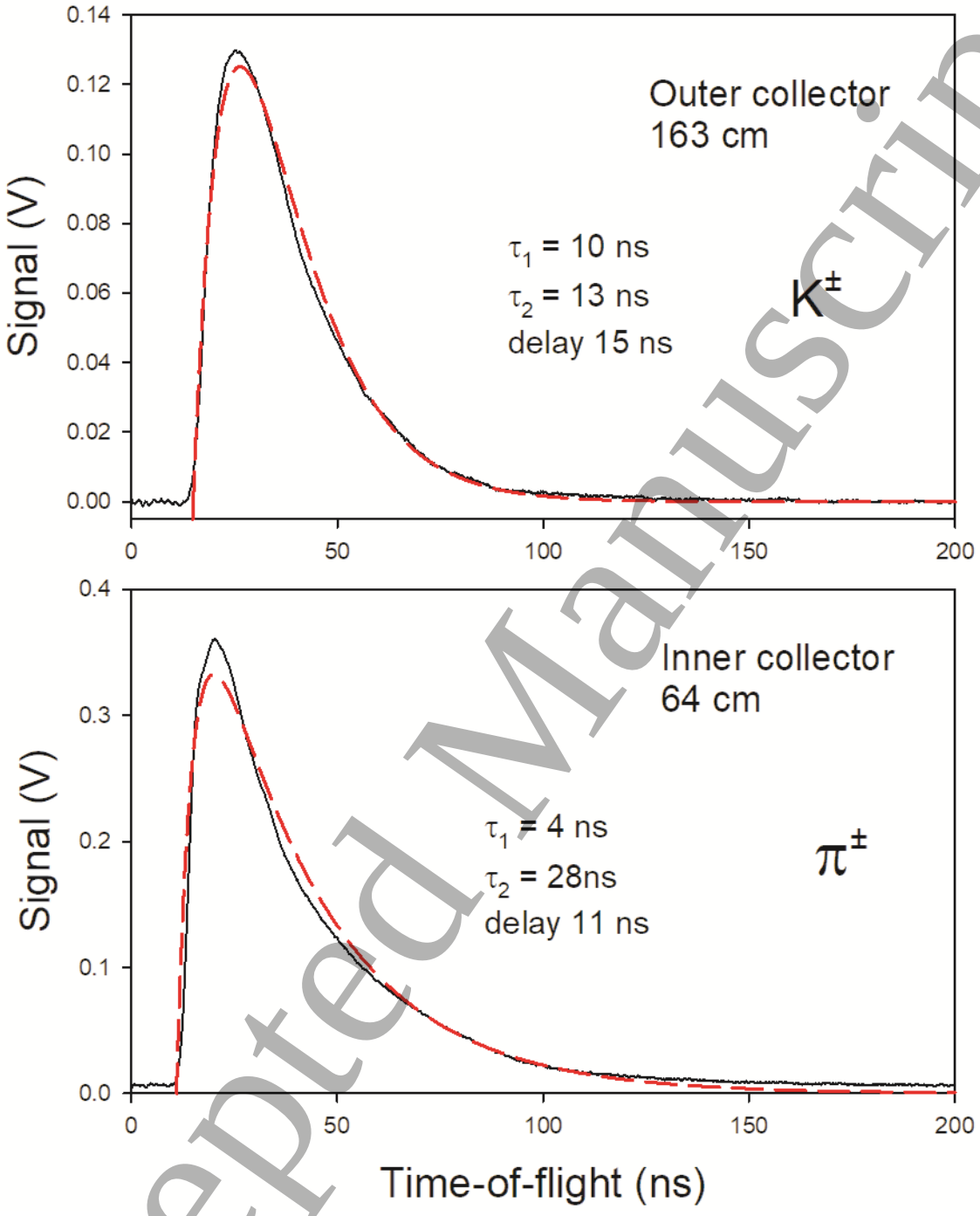

Fig. 7

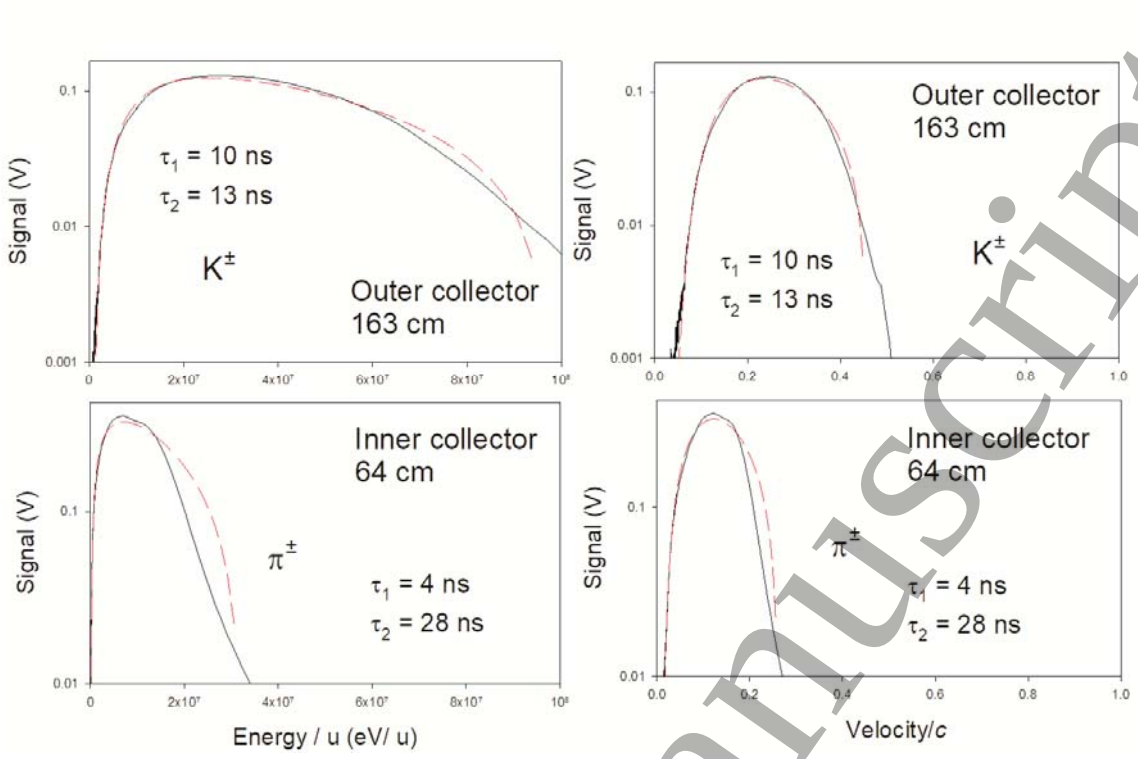

Fig. 8

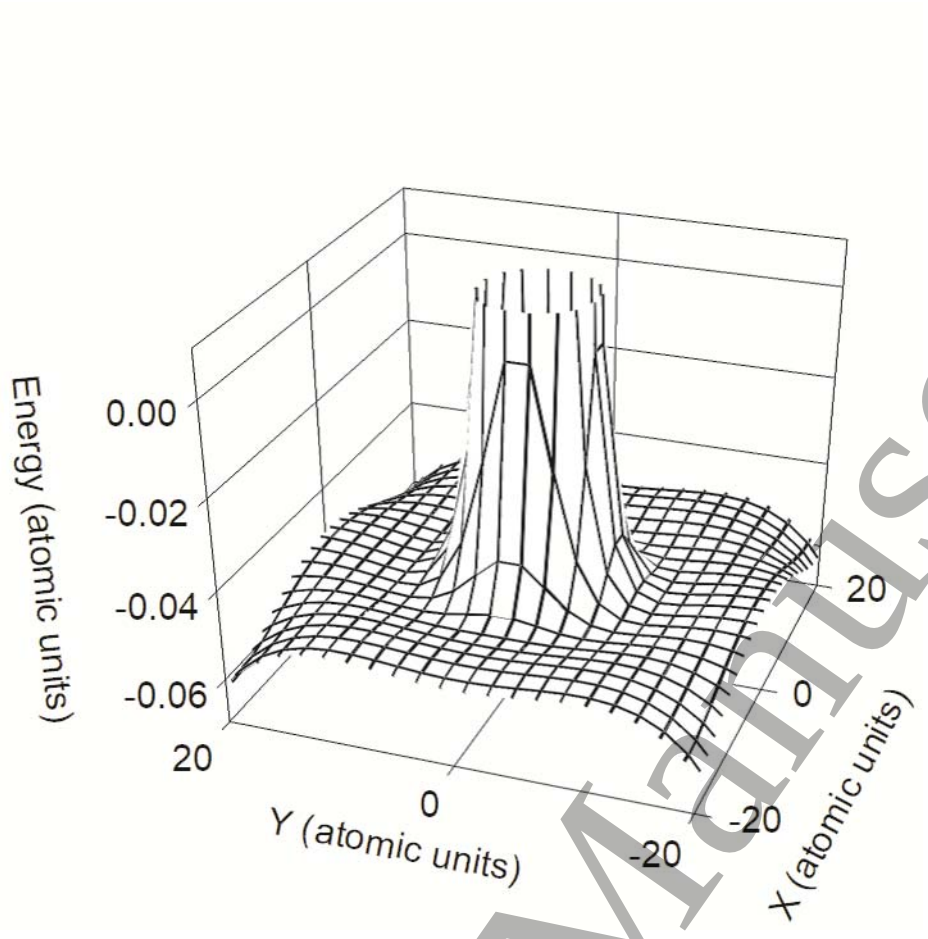

Fig. 9

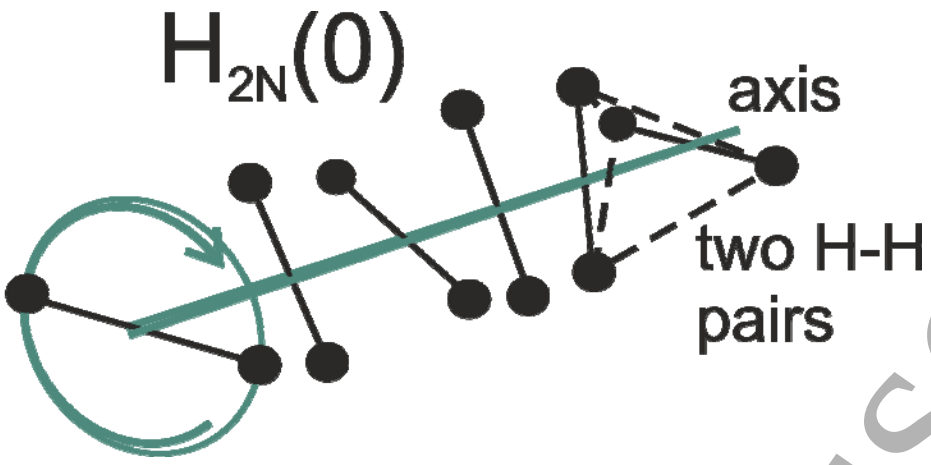

Fig. 10

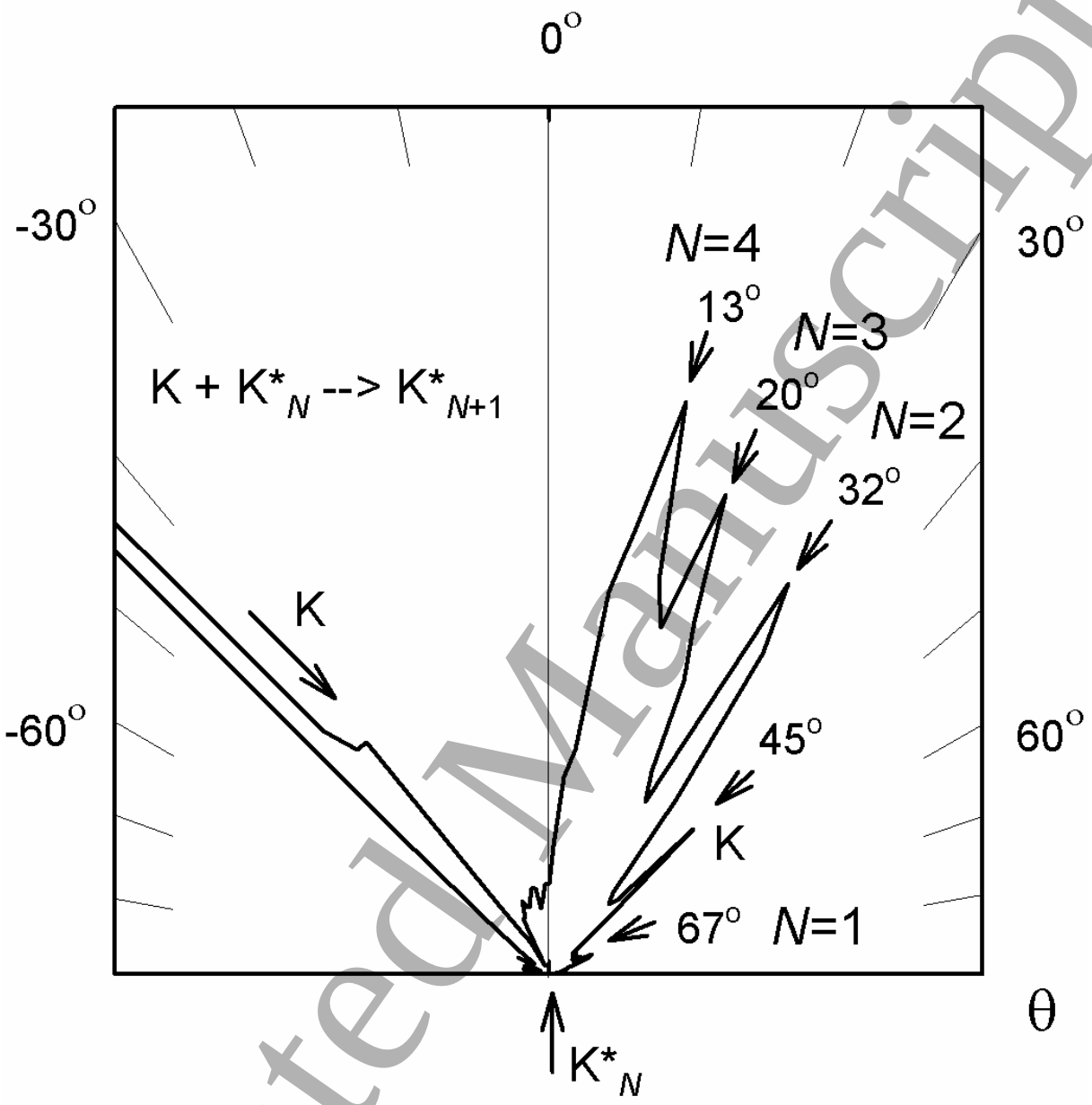

Fig. 11

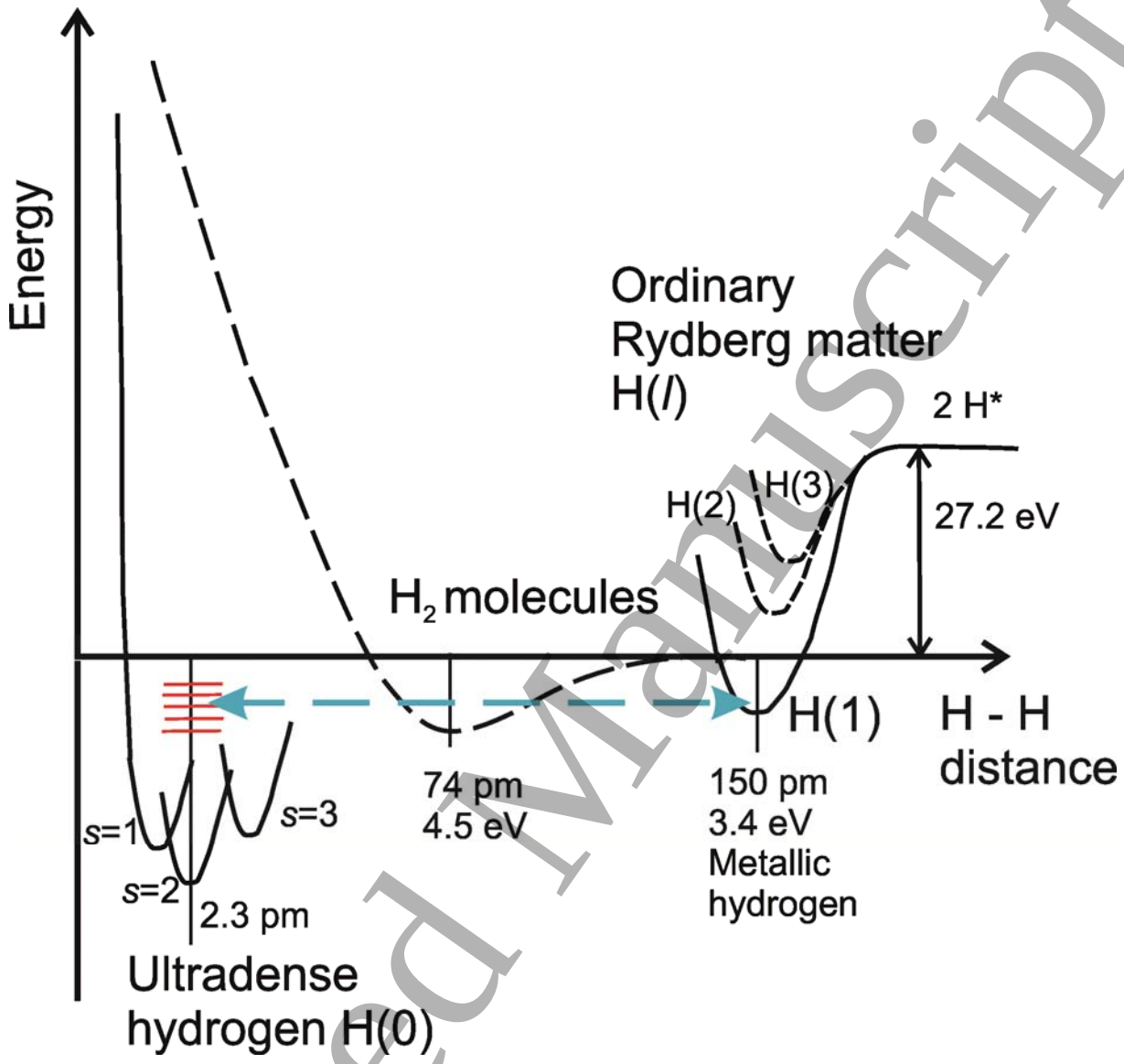

Fig. 12

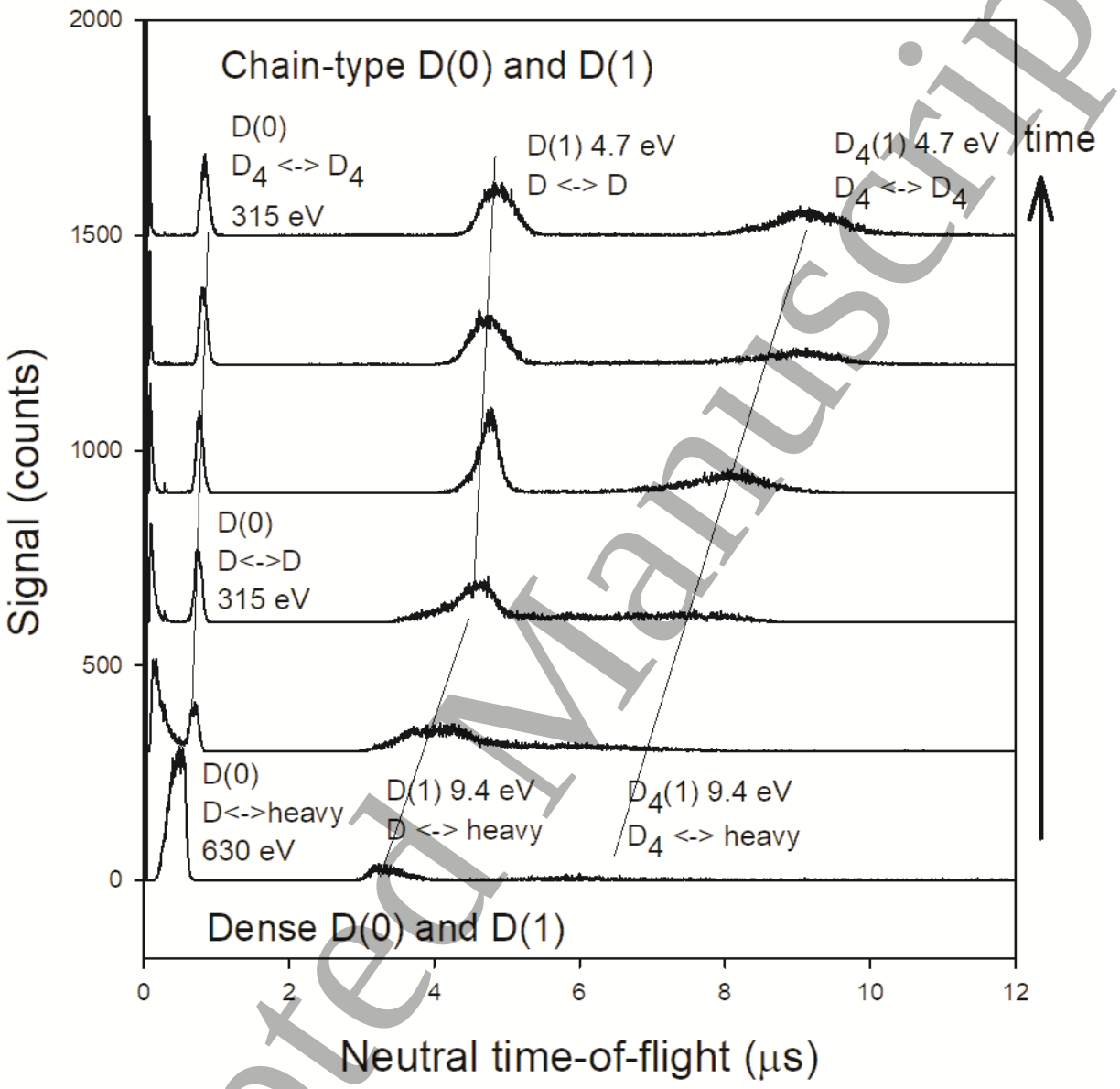

Fig. 13

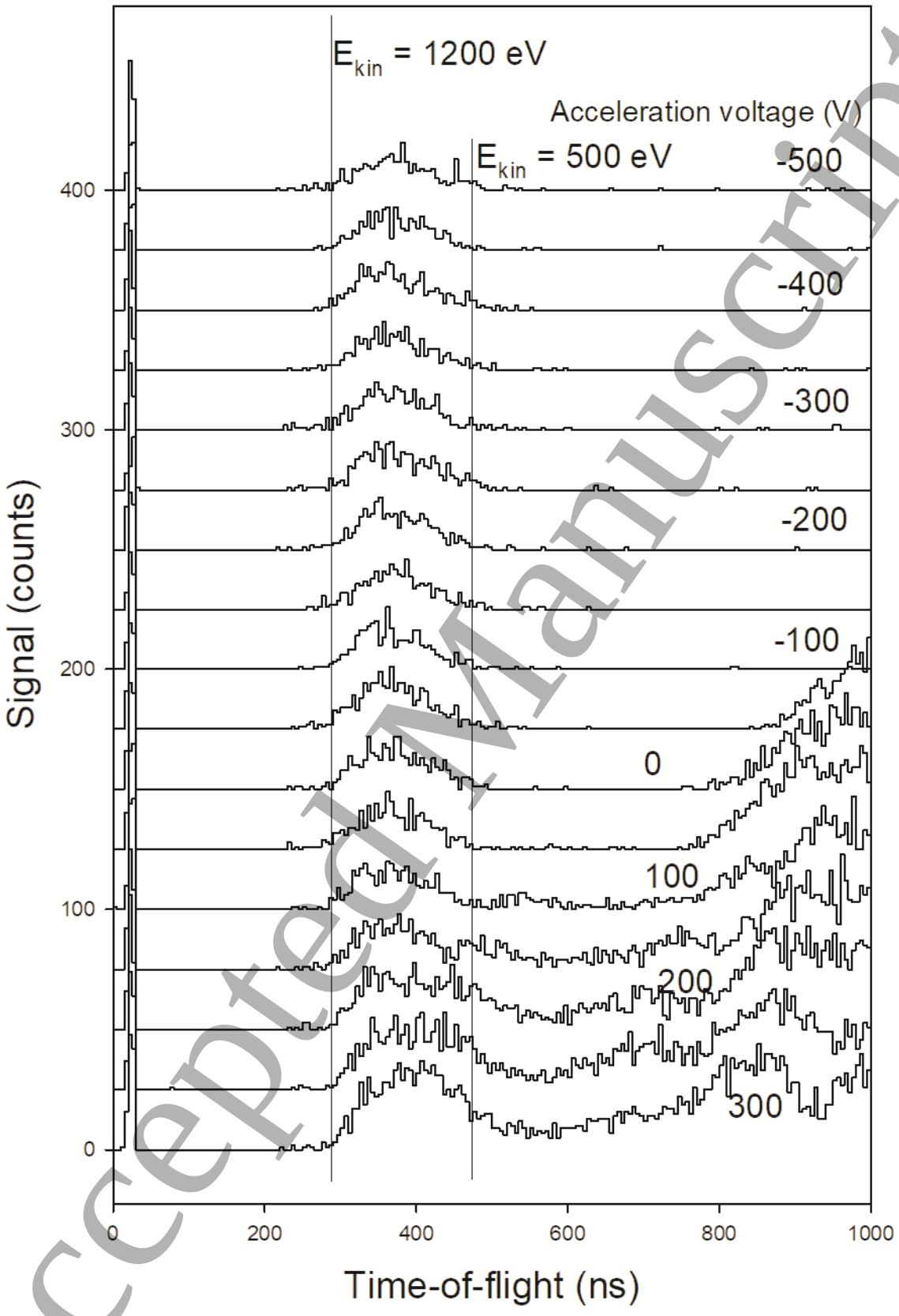

Fig. 14

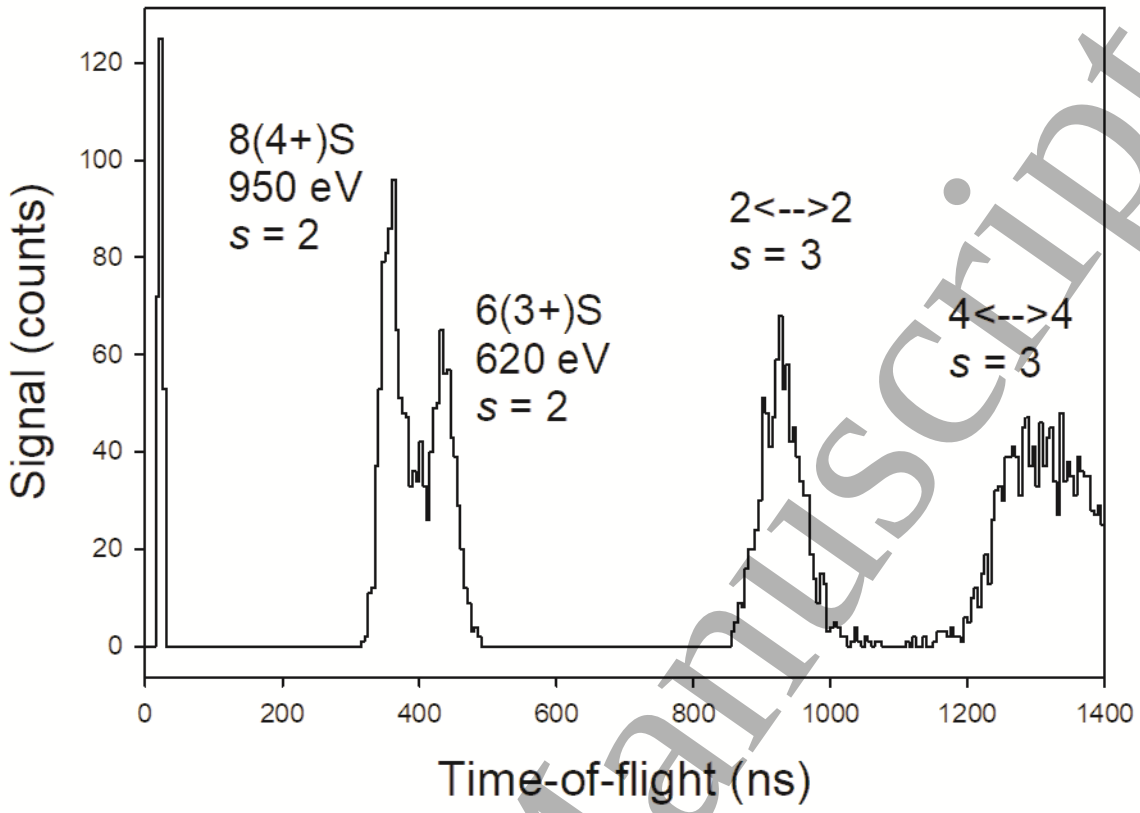

Fig. 15

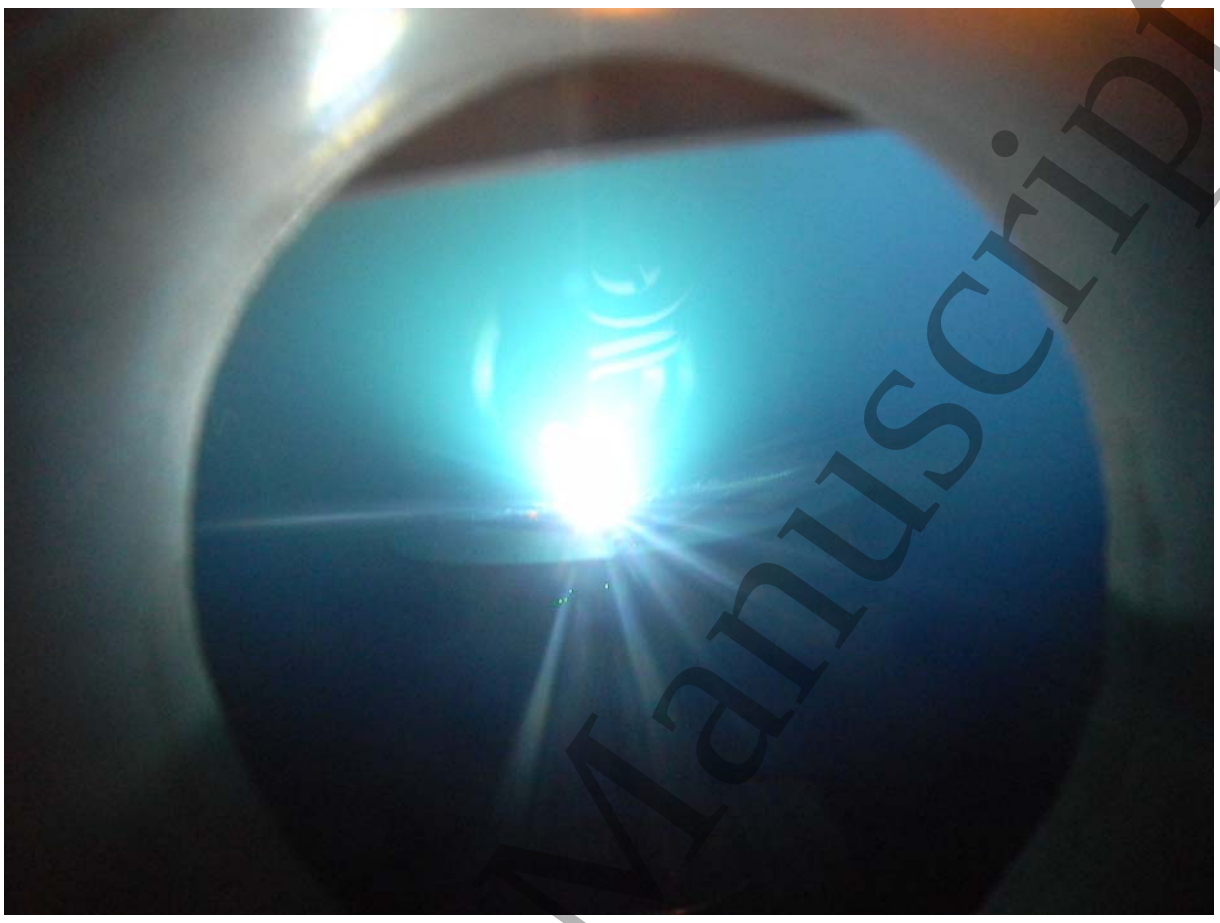

Fig. 16.

Fig. 17. one frame from CIMG00373.mov

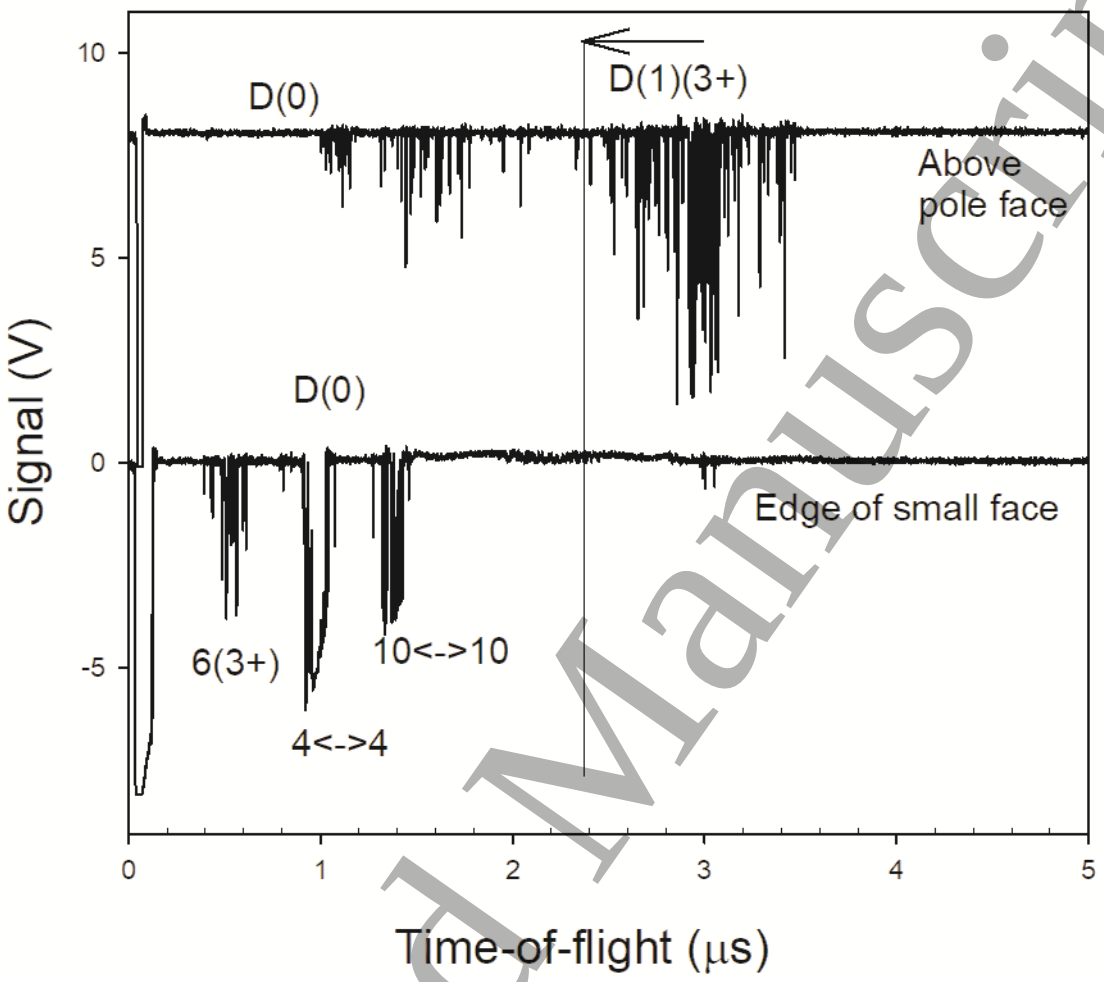

Fig. 18

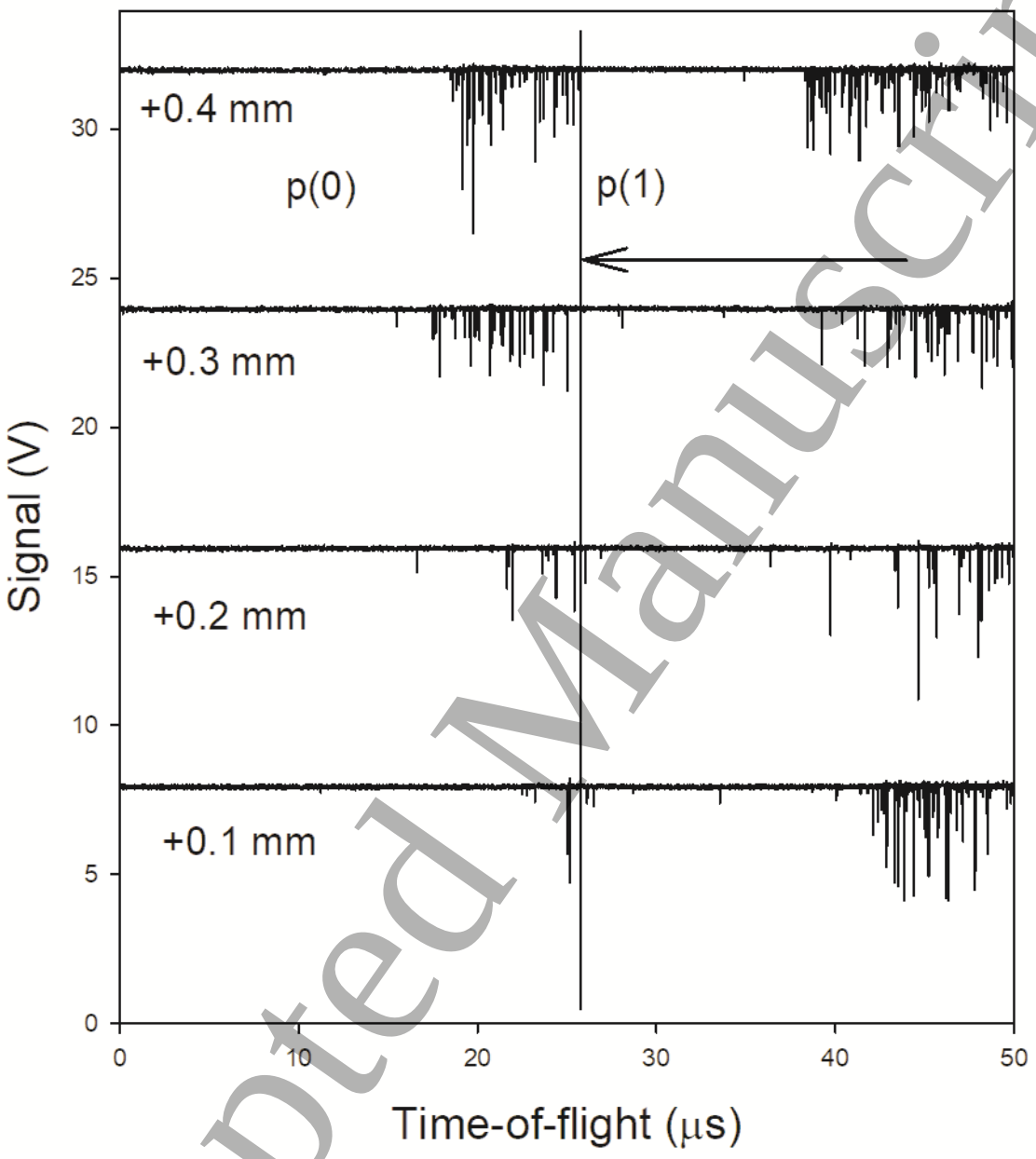

Fig. 19

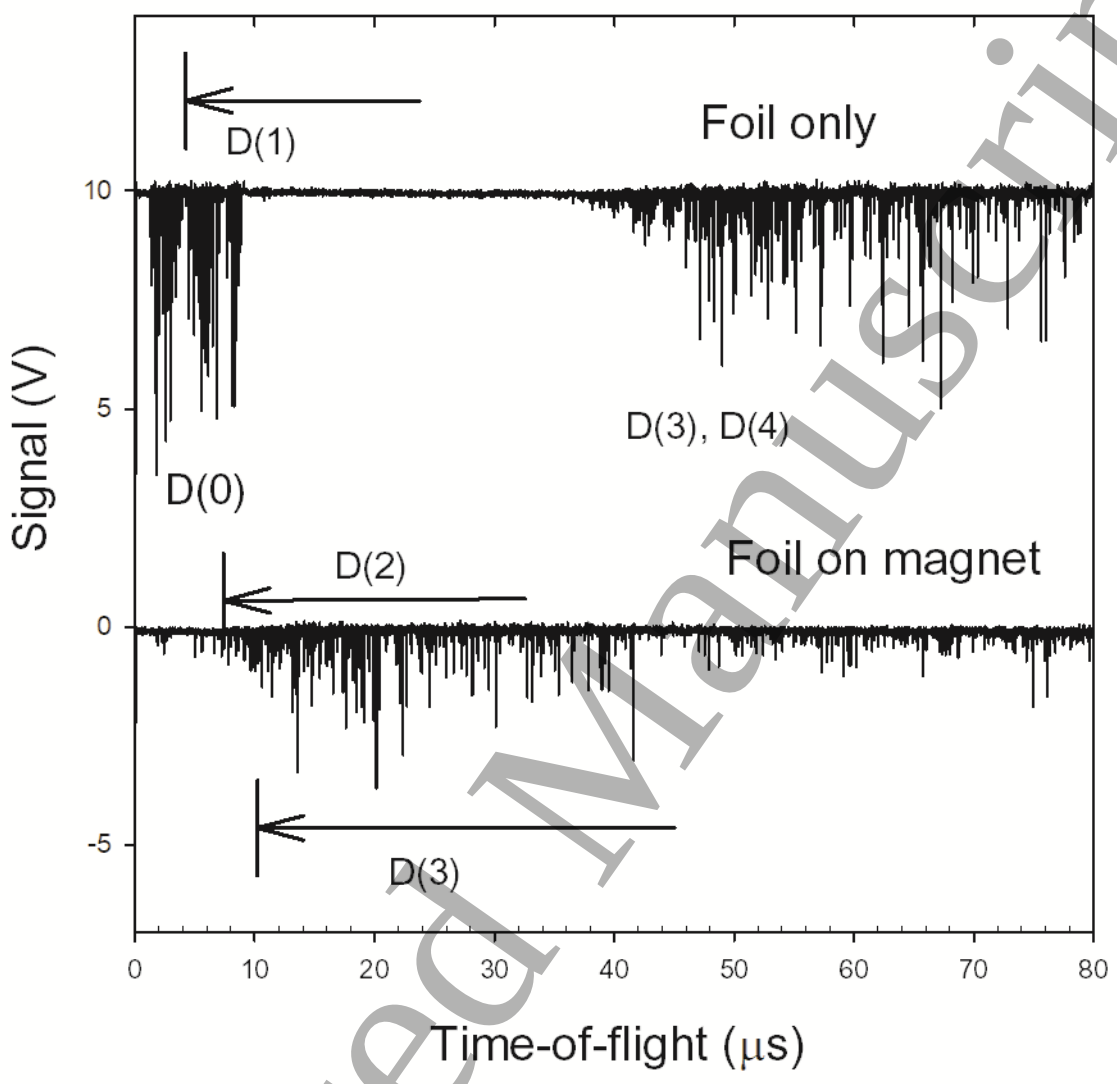

Fig. 20

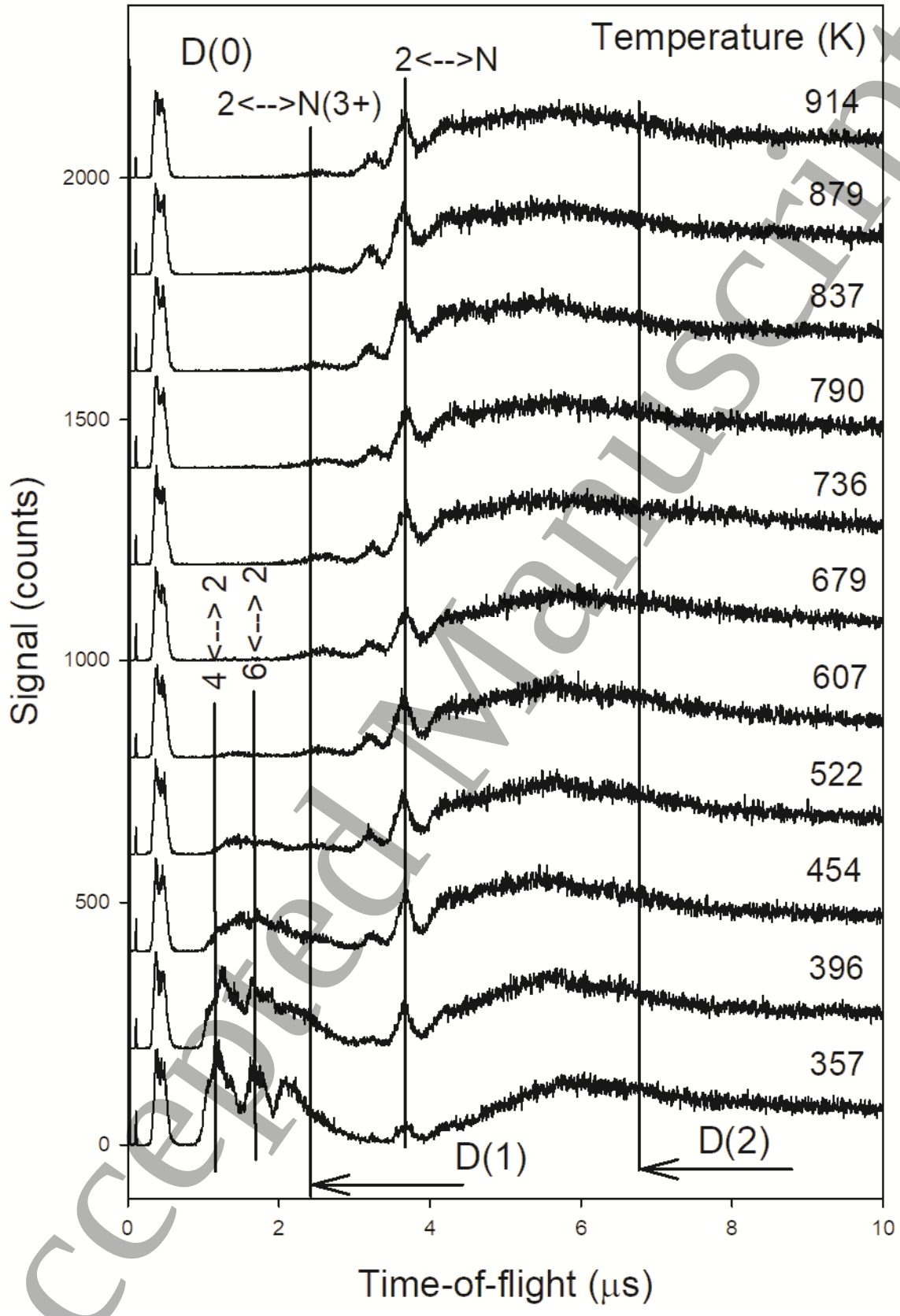

Fig. 21

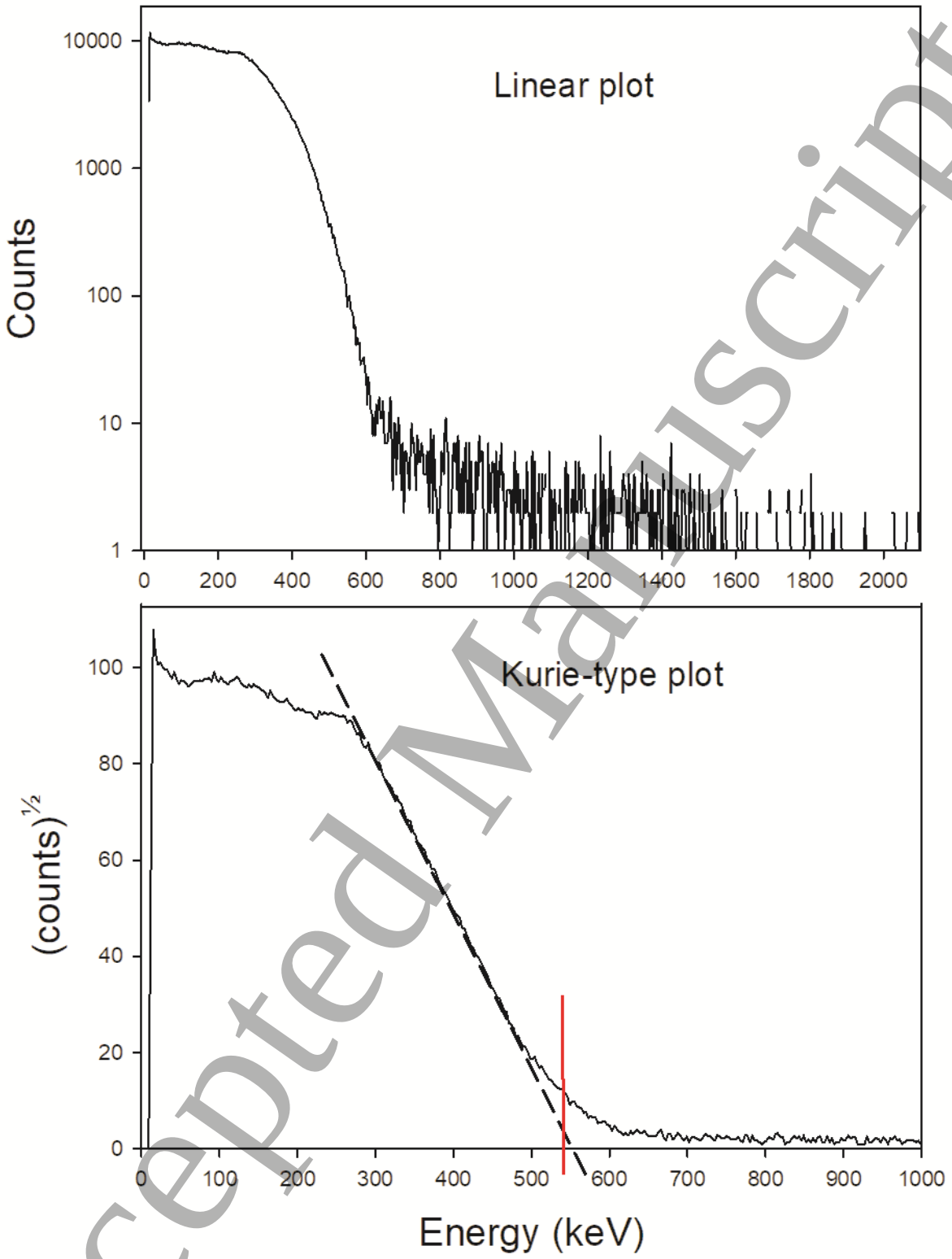

Fig. 22

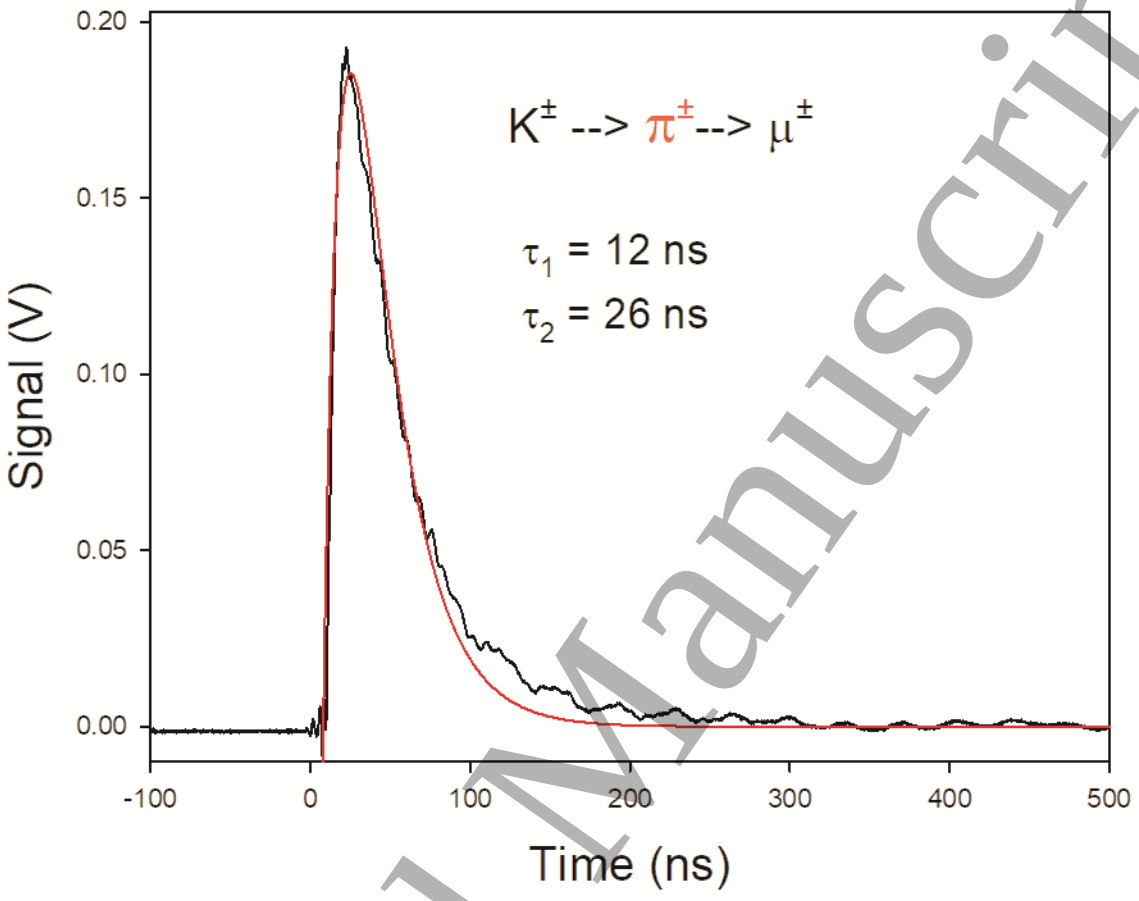

Fig. 23

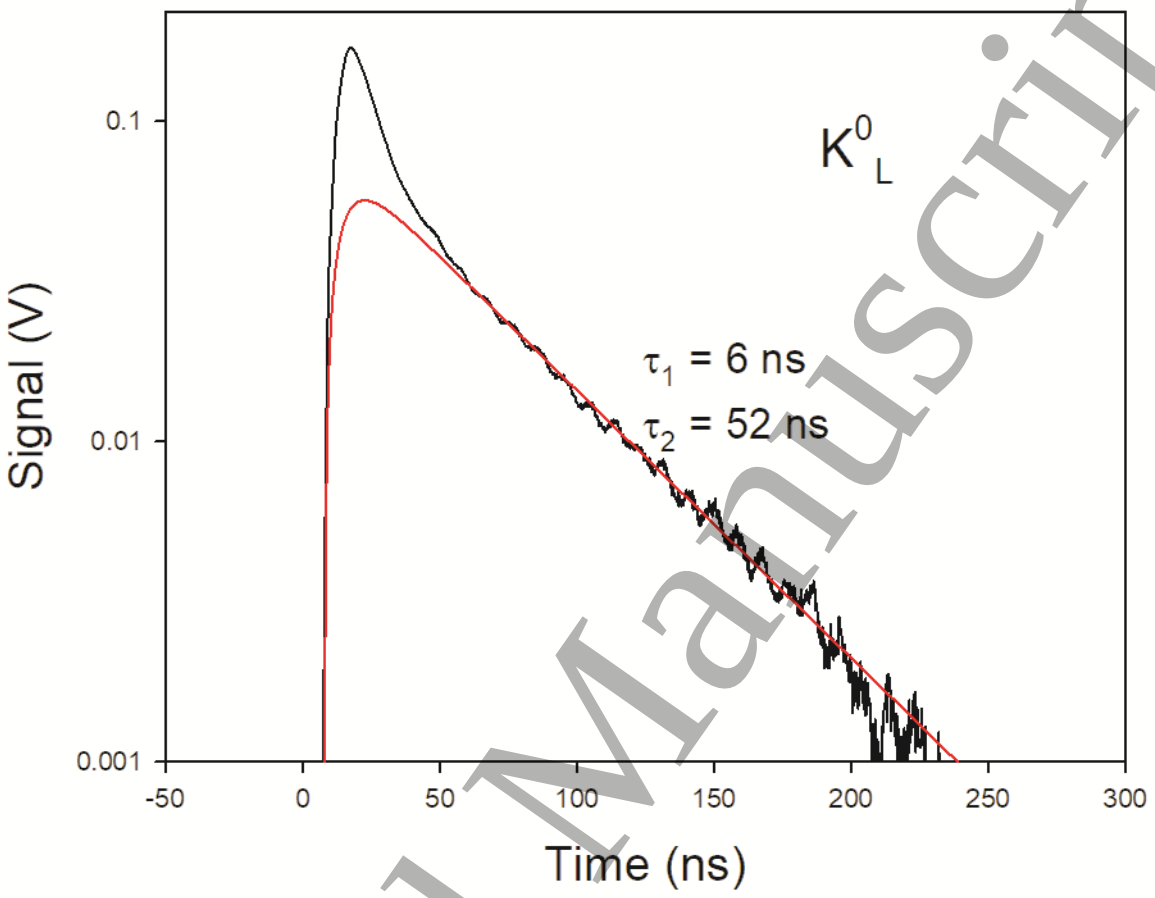

Fig. 24

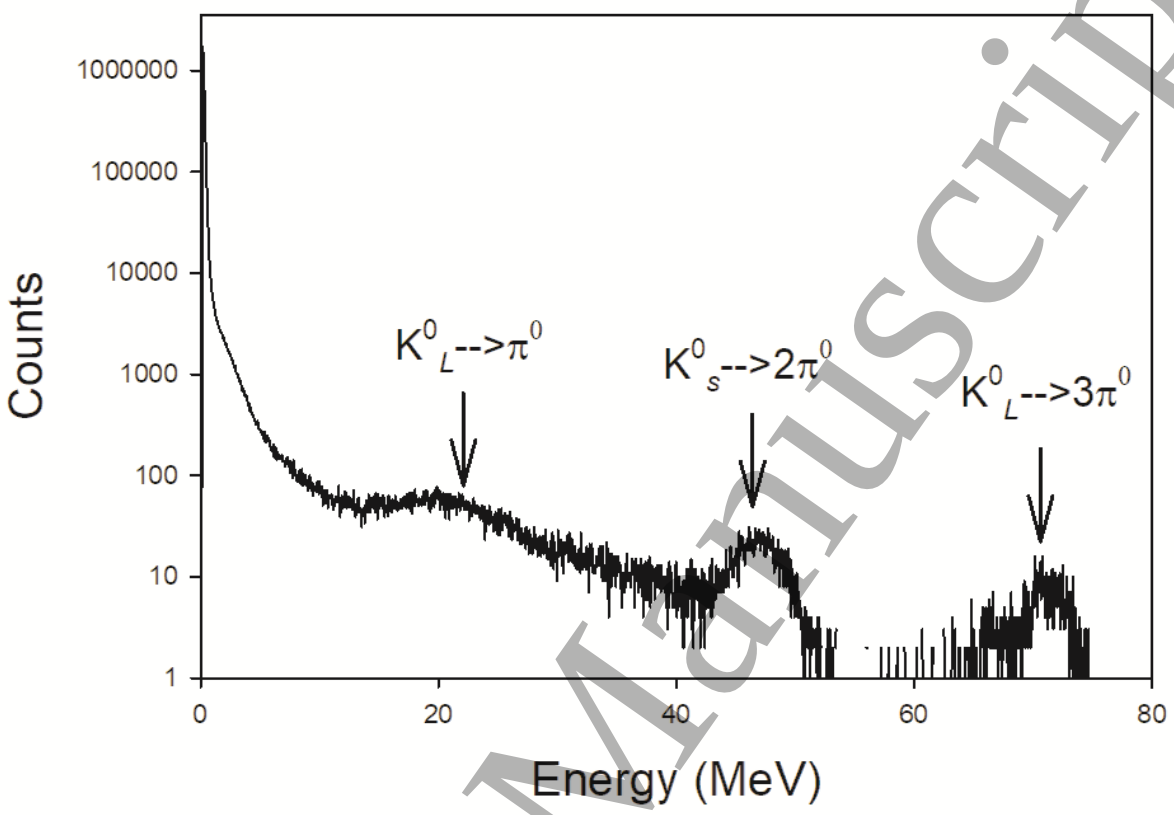

Fig. 25